

2013•2014
FACULTEIT GENEESKUNDE EN LEVENSWETENSCHAPPEN
master in de biomedische wetenschappen

Masterproef

Electrostatic positioning of fluorescent nanodiamonds into nanoscaled arrays using block copolymer-based nanolithography

Promotor :
Prof. dr. Hans-Gerhard BOYEN

Copromotor :
Prof. dr. Milos NESLADEK
dr. Anitha ETHIRAJAN

De transnationale Universiteit Limburg is een uniek samenwerkingsverband van twee universiteiten in twee landen: de Universiteit Hasselt en Maastricht University.



Universiteit Hasselt | Campus Hasselt | Martelarenlaan 42 | BE-3500 Hasselt
Universiteit Hasselt | Campus Diepenbeek | Agoralaan Gebouw D | BE-3590 Diepenbeek

Christopher Freiwald

Proefschrift ingediend tot het behalen van de graad van master in de biomedische wetenschappen



2013•2014
FACULTEIT GENEESKUNDE EN
LEVENSWETENSCHAPPEN
master in de biomedische wetenschappen

Masterproef

Electrostatic positioning of fluorescent nanodiamonds
into nanoscaled arrays using block copolymer-based
nanolithography

Promotor :
Prof. dr. Hans-Gerhard BOYEN

Copromotor :
Prof. dr. Milos NESLADEK
dr. Anitha ETHIRAJAN

Christopher Freiwald

Proefschrift ingediend tot het behalen van de graad van master in de biomedische wetenschappen

Table of Contents

Abbreviations.....	III
Acknowledgement	V
Abstract	VII
Samenvatting	IX
1 Introduction.....	1
1.1 Micelle formation	2
1.2 Analytical tools	3
1.2.1 X-ray Photoelectron Spectroscopy	3
1.2.2 Atomic Force Microscopy	6
1.2.3 Dynamic Light Scattering	6
2 Materials and Methods	7
2.1 Silicon substrate preparation	7
2.2 Silanization of silicon substrates	7
2.3 Preparation of micellar solutions	7
2.4 Dip coating	9
2.5 Oxygen plasma etching	10
2.6 Nanolithographical patterning of the APTES layer.....	10
2.7 Hydrogen plasma etching	10
2.8 Nanodiamond deposition.....	10
2.9 Nanodiamond photoluminescence measurements	11
3 Results and discussion	13
3.1 Silicon substrate cleaning procedure optimization	13
3.2 Silanization of silicon substrates	15
3.2.1 Influence of ultrasonication on APTES layer thickness	15
3.2.2 Influence of curing time on APTES layer thickness	17
3.2.3 Oxygen plasma etching conditions for APTES removal.....	18
3.3 Optimization of the micelle formation for use as etch mask	21
3.4 Wetting behaviour of APTES and silicon oxide.....	24
3.5 Nanodiamond depositing on APTES and silicon oxide.....	24

3.6	Analysis of the nanodiamond photoluminescence	27
4	Conclusion and future prospects	29
	References	31
	Supplemental information	33
	Part 1: Summary of all samples	33
	Part 2: Speed voltage correlation of the dip coating setup	36

Abbreviations

AFM	Atomic Force Microscope
APTES	(3-Aminopropyl)triethoxysilane
BCP	Block Copolymer
CMC	Critical Micelle Concentration
DLS	Dynamic Light Scattering
DMF	Dimethylformamide
ESCA	Electron Spectroscopy for Chemical Analysis
H ₂ O	Water
H ₂ O ₂	Hydrogen peroxide
H ₂ SO ₄	Sulphuric acid
HAuCl ₄	Chloroauric acid
NDs	Nanodiamonds
NV	Nitrogen-vacancy
PS(n)-b-P2VP(m)	Polystyrene(n)-block-poly-2-vinylpyridine(m)
XPS	X-ray Photoelectron Spectroscopy
ZPL	Zero-phonon Line

Acknowledgement

First of all I would like to thank Prof. dr. Hans-Gerd Boyen (Nanostructure Physics group), Prof. dr. Milos Nesladek (Wide Bandgap Materials group), dr. Anitha Ethirajan (BIOSensor group) and the Institute for Materials Research (IMO) for giving me the opportunity to complete my senior practical training in such an inspiring, warm and welcoming environment.

I would like to thank my promotor Prof. dr. Hans-Gerd Boyen for welcoming me in his research team and for his support and guidance during the final chapter of my master's.

I would like to express my gratitude to dra. Tanya Jacobs and drs. Joris Artois for all their support. I could not only count on them for practical assistance in the laboratory, but we also had many interesting and constructive conversations regarding the research. I would also like to thank them again for all the measurements they performed for my thesis.

From the Wide Bandgap Materials group I would like to thank my copromotor Prof. dr. Milos Nesladek and dra. Elena Gjorgievska for providing the fluorescent nanodiamond particles and for their expertise. I would also like to thank dr. Emilie Bourgeois for performing the photoluminescence measurements of the nanodiamonds and for helping me with the interpretation of the acquired data.

From the BIOSensor group I would like to thank my copromotor dr. Anitha Ethirajan for her advice regarding the micellar approach.

I would like to thank my fellow students Lien Callens, Mandy Berden and Sören Kuypers for all their support and for offering a moment of recreation during the lunch breaks. Mandy and Sören I also would like to thank for assisting me with the dynamic light scattering measurements. Special thanks go out to Lien for allowing me to assist with her research and for making it possible to continue my research during the recovery from my knee surgery. Every morning of this period she picked me up at my apartment and drove me back home in the evening.

All the technical personal of the institute I would like to thank for their assistance, especially Johnny Baccus.

Albert Einstein once said "If you can't explain it simply, you don't understand it well enough." This being said, I would like to thank my promotor Prof. dr. Hans-Gerd Boyen again. He took the time to explain to me some of the complex theory behind observations and experimental setups (which often involved quantum physics) in such a way that even I could understand it. This proves that he is a real expert in his field who truly understands his matter.

Abstract

The controlled and precise positioning of nanoscaled particles on a substrate is one of the key challenges for the design of new functional surfaces used in photonics, optoelectronics, (bio)chemistry and (bio)sensing.

The aim of this master thesis was to lay the foundations for the development of nanoscaled arrays of fluorescent nanodiamond particles, by electrostatic-guided positioning using block copolymer based nanolithography.

A novel five step technique proposed by Li Wang et al was adapted to create the nanoscaled arrays. First a substrate is covered with a positively charged layer. During the next steps this layer is partially removed by using a monolayer of block copolymer micelles as an etch mask. After removal of the remaining micelles, the substrate is submerged in a dispersion of negatively charged nanoparticles. Finally, electrostatic forces guide the negatively charged particles to the positively charged islands where they bind to the surface.

During this master thesis the potential of this technique for the controlled positioning of highly fluorescent nanodiamond particles was analysed by carefully studying each of the five required preparational steps. It could be demonstrated that, when referring to individual steps, all components of the technique work well. However, due to severe problems related to the formation of the micellar etch mask, it was not possible to link all components together within the timescale of this thesis.

However, once the problem regarding the micellar approach has been tackled, all pieces of the puzzle should come together to create a well-defined array of highly fluorescent nanodiamond particles. This is the foundation on which an enormous range of applications could be build in the future. These applications could span from controlled cell growth to DNA-sensors or even quantum computing. However, during this thesis mainly applications for (bio)sensing have been kept in mind.

Samenvatting

Eén van de grootste uitdagingen voor de ontwikkeling van nieuwe functionele oppervlakken die toepassingen hebben binnen de fotonica, opto-elektronica, (bio)chemie en (bio)sensing, is het nauwkeurig positioneren van nanopartikels op een substraat.

Het doel van deze master proef was om de basis te leggen voor de ontwikkeling van geordende arrays van fluorescente nanodiamanten op nanoschaal door elektrostatisch geleide positionering. Dit door middel van gebruik te maken van nanolithografie gebaseerd op blokcopolymeer micellen.

Voor de vorming van de arrays op nanoschaal werd een recent, door Wang et al. voorgestelde vijf-stappen techniek aangepast. Tijdens de eerste stap wordt het substraat bedekt met een positief geladen laag. In de volgende stappen wordt deze laag gedeeltelijk verwijderd door een monolaag van blokcopolymeer micellen te gebruiken als masker tijdens het plasma etsen. Na het verwijderen van de overgebleven micellen wordt het substraat ondergedompeld in een dispersie van negatief geladen nanopartikels. Uiteindelijk zullen de negatief geladen partikels door elektrostatische krachten worden geleid naar de positief geladen eilanden en daar binden aan het oppervlak.

Tijdens deze masterproef werd iedere voorbereidende stap van deze techniek grondig bestudeerd om de potentiële toepassing van deze techniek op het gecontroleerd positioneren van sterk fluorescerende nanodiamanten te onderzoeken. Het kon worden aangetoond dat iedere stap van de techniek op zich goed werkt. Door problemen met de vorming van de micellen, nodig voor het gebruik als masker tijdens het etsen, konden alle componenten echter niet samengevoegd worden binnen het tijdschema van deze master proef.

Eens de problemen met het vormen van micellen zijn opgelost, zouden alle puzzelstukken moeten samenvallen om een goed gedefinieerde array van sterk fluorescerende nanodiamanten te kunnen vormen. Dit vormt de basis waarop in de toekomst een brede waaier aan toepassingen zou kunnen worden ontwikkeld. Deze toepassingen kunnen reiken van gecontroleerde celgroei tot DNA-sensoren of zelfs kwantum computing. Voor deze master proef werden voornamelijk toepassingen voor (bio)sensing in het achterhoofd gehouden.

1 Introduction

Designing new functional surfaces is a hot topic in a broad variety of research fields like optoelectronics, photonics, (bio)chemistry and (bio)sensing. Especially the controlled positioning of nanoscaled structures such as nanoparticles in predefined arrangements is still one of the key challenges. Research of Li Wang et al. shows that it is possible to use the self-assembling properties of block copolymer micelles in combination with nanolithography to electrostatically bind gold nanoparticles to a surface in a controlled manner⁽¹⁾. The aim of this master thesis was to adapt and optimize the above mentioned technique to arrange fluorescent nanodiamond particles in well-defined arrays.

Nanodiamonds have a strong potential for future applications due to their fluorescent properties. By artificial incorporation of specific point defects in the nanodiamond it is possible to induce so called "nitrogen-vacancy centres"⁽²⁾. The fluorescence of nitrogen-vacancy (NV) centres can be reduced by a process called "quenching". Quenching can be induced by the binding of a molecule to the nanodiamond⁽³⁾. Registering these changes in the fluorescence of the nanodiamonds forms the foundation for the development of a variety of (bio)sensors.

Developing a nanoscaled array of these fluorescent nanodiamond particles is the first step towards the development of nanoscaled (bio)sensors which will surpass the density of current micro- or even millimetre-based technologies by many orders of magnitude.

The aim of this master thesis was to use block copolymer-based nanolithography to electrostatically position fluorescent nanodiamonds into nanoscaled arrays of controllable dimensions.

In order to achieve this goal a five step technique was used as described in Figure 1.

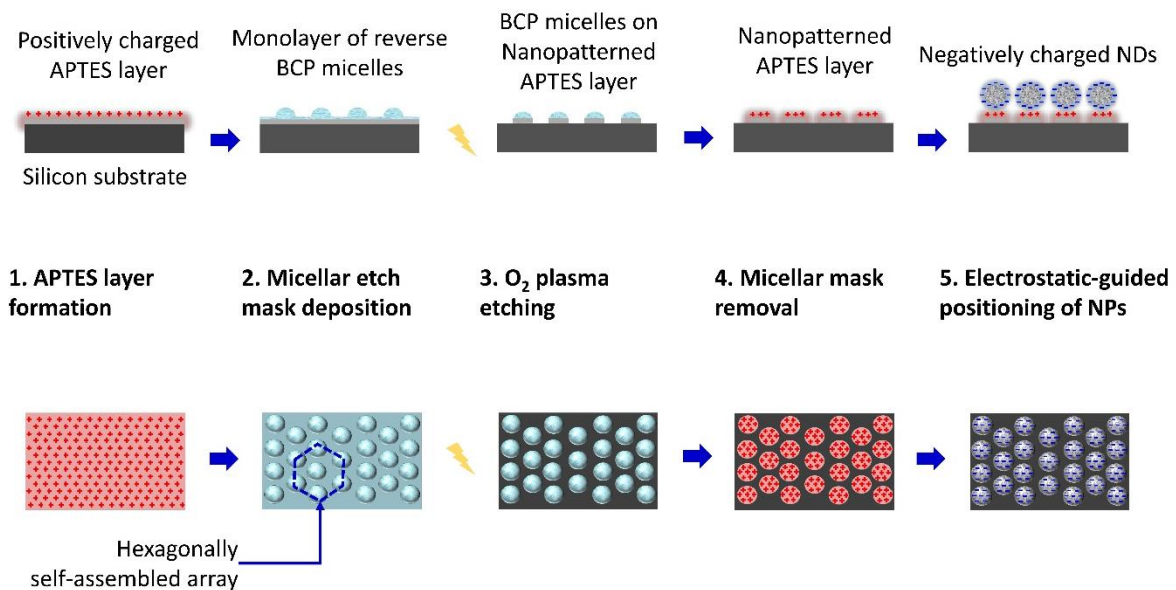


Figure 1: Schematic process for the formation of APTES nanopatterns by block copolymer-nanolithography (steps 1-4) and the electrostatic guided-positioning of gold nanoparticles (step 5). (APTES = (3-Aminopropyl)triethoxysilane, BCP = Block co-polymer, NDs = Nanodiamonds)

First a silicon substrate is coated with (3-Aminopropyl)triethoxysilane (APTES). This positively charged layer will later on allow the attraction and electrostatic binding of the negatively charged nanodiamond particles.

Next a monolayer of block copolymer micelles is applied. This micellar array will act as a mask during the oxygen plasma etching (step 3).

After removal of the remaining micellar mask in step four, a nanoscaled pattern of positively charged APTES islands remains. The array of these islands corresponds to the original micellar pattern of the mask.

Finally the substrate is submerged in a colloidal dispersions of negatively charged nanodiamond particles. The electrostatic forces guide and bind the nanodiamond particles to the APTES islands.

1.1 Micelle formation

Micelles are (spherical) aggregates of amphiphilic molecules dispersed in a polar solvent. Amphiphilic molecules consist of two parts, a hydrophilic (polar) and a hydrophobic (nonpolar) part as shown in Figure 2A. The behaviour of amphiphilic molecules in a solvent is a thermodynamically driven process, in which the system tries to minimize the Gibbs free energy. Equation 1 gives the change in Gibbs free energy at a given pressure and temperature.

$$\Delta G(p, T) = \Delta H - T\Delta S$$

Equation 1: Gibbs free energy. $\Delta G(p, T)$ is the change in Gibbs free energy at a given pressure (p) and temperature (T), ΔH is the change in enthalpy, T is the temperature in K and ΔS is the change in entropy.

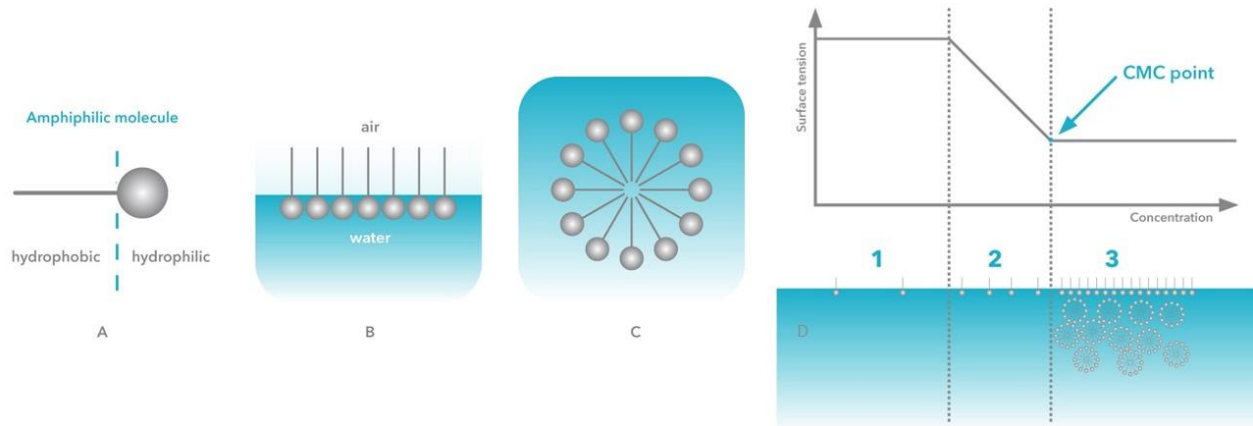


Figure 2: Amphiphilic molecules in a polar solvent. A: Schematic representation of an amphiphilic molecule with a hydrophobic part (left) and a hydrophilic part (right). B: Amphiphilic molecules at a water-air interface. C: Amphiphilic molecules arranged in a micelle⁽⁴⁾.

There are two ways to decrease the Gibbs free energy. Either decrease the enthalpy or increase the entropy. In order to reduce the enthalpy of the system, the hydrophobic part of the molecules avoids to be in contact with the polar solvent. This reduces the Gibbs free energy of the system and explains the favoured arrangements shown in Figure 2B-C. Although these arrangements are favoured the system is

still dynamic, meaning that the amphiphilic molecules are constantly in motion and some molecules may temporarily enter the solvent completely.

At low concentrations, the presence of the amphiphilic molecules at the surface will have no noticeable influence on the surface tension. With increasing concentration the surface tension decreases as shown in Figure 2D (Note that the concentration is plotted on a logarithmic scale in order to get a linear decrease of the surface tension.). At a given concentration, the surface becomes saturated and any additional amphiphilic molecules must enter the solvent. From this point on the surface tension remains constant. This concentration is called the Critical Micelle Concentration (CMC). From this concentration on and higher, any additional amphiphilic molecules are incorporated in micellar aggregates.

The technique described in this master thesis uses reverse micelles. Reverse micelles follow the same principal as regular micelles, but instead of dissolving the amphiphilic molecules in a polar solvent, they are dissolved in a non-polar solvent. In this way the amphiphilic molecules will form spherical aggregates where the hydrophilic part of the molecules is centred at the core of the micelle to avoid being in contact with the hydrophobic solvent. The hydrophobic part of the molecules forms a protective shell that shields the hydrophilic core.

1.2 Analytical tools

Various analysis methods were used to investigate the molecular and morphological properties during the different steps of this master thesis.

1.2.1 X-ray Photoelectron Spectroscopy

X-ray Photoelectron Spectroscopy (XPS) also known as Electron Spectroscopy for Chemical Analysis (ESCA) is a highly sensitive surface analysis technique capable of providing qualitative and quantitative information of the most upper few atomic layers of a surface⁽⁵⁾.

XPS is based on the photoelectric effect described by Albert Einstein in 1905. The photoelectric effect describes a process by which electrons are emitted from a surface when irradiated with photons. In order to emit an electron, the energy of the incident photon must be higher than the electron binding energy of the irradiated surface. The energy of a photon is directly correlated to its frequency and inversely correlated to its wavelength (Equation 2).

$$E_p = h\nu = h \frac{c}{\lambda}$$

Equation 2: Energy of a photon. h is Planck's constant, ν is the frequency of the photon, C is the speed of light and λ is the wavelength of the photon.

When one looks at the electromagnetic spectrum, the wavelength of infrared radiation is too long and therefor the energy is not sufficient to induce photoelectron emission. The wavelength of visible and ultraviolet light is shorter and the energy becomes high enough to emit photoelectrons of materials with

a low electron binding energy. X-rays and gamma-rays have even shorter wavelengths and carry sufficient energy to emit photoelectrons in all materials (*Figure 3*). Because X-rays can easily be produced and are safer to handle than gamma-rays, they are the preferred choice for photoelectron spectroscopy.

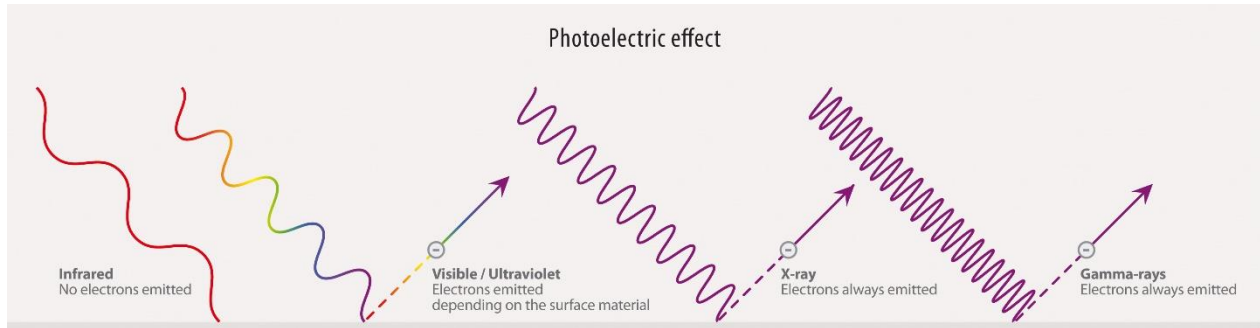


Figure 3: Photons with increasing energy (from left to right) can induce photoelectron emission when their energy is larger than the work function of the irradiated surface.

Figure 4 shows the most essential components of an X-ray photoelectron spectrometer. These components are: an ultrahigh vacuum chamber [1], an X-ray source [2], an electron energy analyser [3] and a data processing system [4].

The X-ray source has a heated filament that functions as cathode (-) and an anode (+) of a certain material, most often aluminium or magnesium. When a high voltage is applied, the filament bombards the anode with electrons. These incoming electrons collide with the atoms of the anode material and excite electrons to higher energy states. Electrons of higher energy relax to lower energy levels and release their excess energy in the form of X-rays.

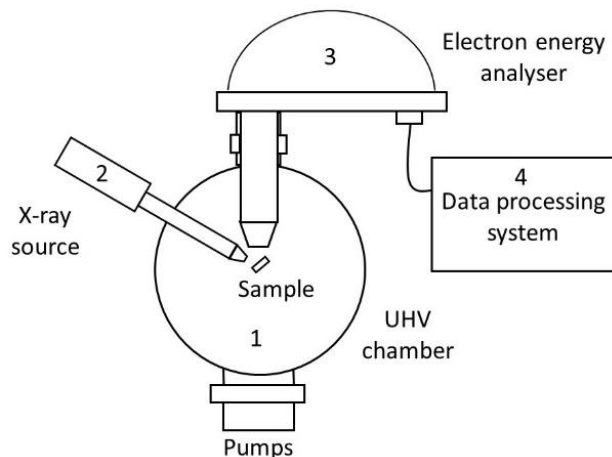


Figure 4: Schematic of an X-ray photoelectron spectrometer setup.

The X-rays, optionally, pass through a monochromator system onto the sample. There they induce electron emission according to the photoelectric effect described above. The emitted photoelectrons pass through an electron energy analyser. This analyser consists of an entrance and exit slit of certain dimensions and two hemispherical electrodes. The outer electrode has a negative charge and the inner a positive charge, in this way only electrons with a certain kinetic energy follow the right trajectory too pass through the exit slit. Electrons with a kinetic energy that is too high collide with the outer electrode, electrons with a kinetic energy that is too low are collected by the inner electrode. In this way the number of electrons with a distinct kinetic energy can be counted by an electron detector. By repetitively increasing the potential of the hemispherical electrodes, scan of electrons with increasing kinetic energy are obtained.

Once the kinetic energy of the photoelectrons is determined, the original electron binding energy can be calculated by *Equation 3*. To obtain the original binding energy of the photoelectron, the measured kinetic energy and the work function of the spectrometer (which is characteristic for the setup) are subtracted from the known photon energy of the X-rays ⁽⁶⁾.

$$E_B = E_p - E_k - \phi$$

Equation 3: Binding energy of photoelectron. Where E_B is the electron binding energy, E_p is the energy of the incident photon, E_k is the kinetic energy of the photoelectron and ϕ is the work function of the spectrometer ⁽⁶⁾.

Each element known to man has its own characteristic set of XPS peaks at distinct electron binding energies, corresponding to the different electron orbitals of the involved atoms. This allows the identification of each element on the surface of the analysed sample.

The high surface sensitivity of XPS derives from the intense inelastic scattering of electrons within a material. If an electron travels through a material it can undergo inelastic collisions with other electrons. During an inelastic collision the electrons lose some of their kinetic energy and can only be detected at low kinetic energies. These electrons form the background of the XPS spectra. The distance an electron can travel through a material without scattering, and thus without losing part of its kinetic energy, is called the mean free path. Figure 5 shows the dependence of the mean free path on the kinetic energy of the electrons. The best surface sensitivity is reached by bringing the kinetic energy of the electrons to about 80 eV. This is where the curve has its minimum and thus the lowest mean free path. The lower the mean free path, the lower the number of atomic layers the electrons can travel before undergoing inelastic scattering. Thus the lower the information depth or the higher the surface sensitivity.

Because this thesis aims at studying the properties of molecular layers within the range of a few nanometres, XPS is due to its high surface sensitivity the ideal tool to do so.

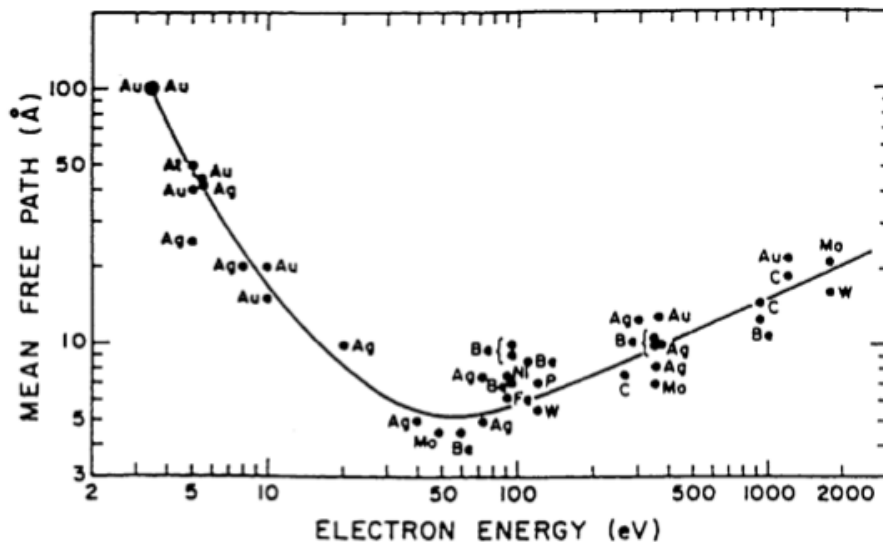


Figure 5: The universal curve for inelastic mean free paths, versus electron kinetic energy (eV)⁽⁵⁾.

1.2.2 Atomic Force Microscopy

Atomic Force Microscopy (AFM) is a powerful tool for imaging surface structures within the range of angstroms to micrometres. The AFM uses a microscopically fine tip to interact with the surface through different short-range forces such as Van der Waals force, dipole-dipole interactions and electrostatic forces (Figure 6). This allows the use of AFM for imaging of almost any kind of surface, including semiconducting or non-conducting materials as well as soft matter⁽⁷⁾.

AFM is a type of scanning probe microscopy. For this type of microscopy an image is obtained by scanning the surface with an AFM tip that is mounted on a cantilever. While scanning, the tip is in close proximity of the surface and will interact with it due to the forces mentioned above. This results in deflection of the cantilever. A laser beam is reflected by the cantilever onto a photodiode. The photodiode detects the deflection of the cantilever and sends a signal to the piezo-electric stage via a feedback loop. In this way the distance between the tip and the surface of the sample is kept constant by changing the height of the stage. The changes in height are registered to create an image of the sample.

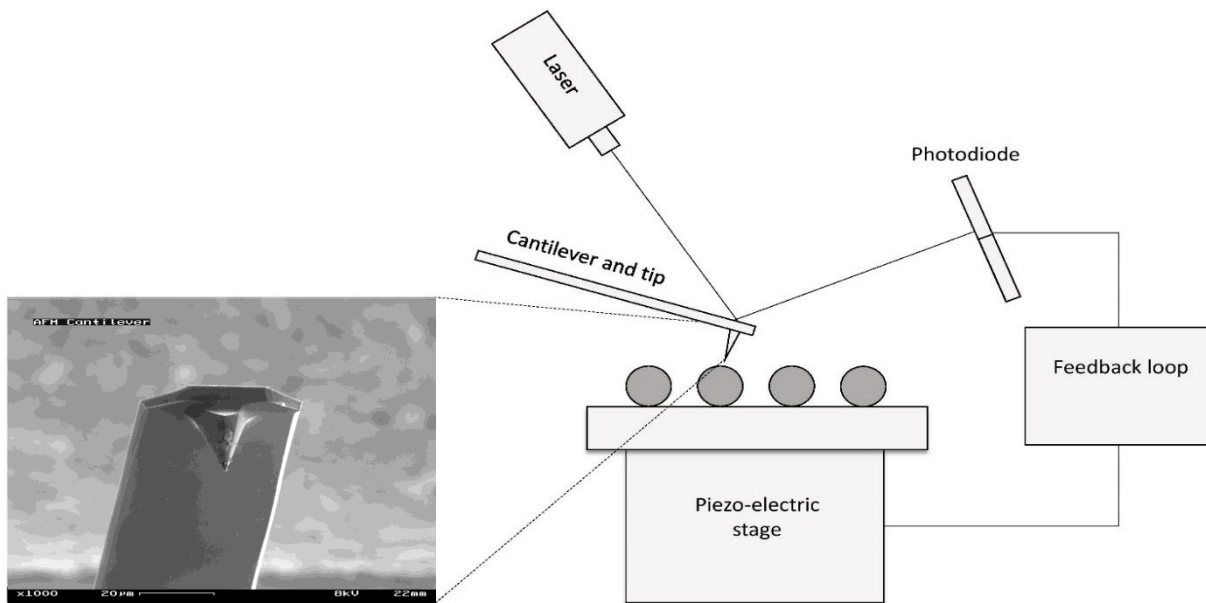


Figure 6: Schematic of an AFM setup (right) and electron microscopic image of AFM cantilever and tip (left)⁽⁸⁾.

1.2.3 Dynamic Light Scattering

Dynamic Light Scattering (DLS) also known as Photon Correlation Spectroscopy or Quasi-Elastic Light Scattering is a technique that can be used to determine the size of micelles, emulsions, nanoparticles, or colloids. For this technique a laser beam is sent through the sample and the scattered light is detected at a certain angle. The constant movement of the dispersed particles results in fluctuations of the scattered light intensity which contains information about the size of the particles. Using an autocorrelation function it is possible to derive this information⁽⁹⁾.

2 Materials and Methods

2.1 Silicon substrate preparation

N-type silicon wafers (diameter 100 mm \pm 0.5 mm, thickness 525 μ m \pm 25 μ m, orientation 111 \pm 0.5°) were obtained from Neyco s.a. (Paris, France). The wafers are phosphorus doped (resistivity 0.1-1.0 Ω cm) and have one polished and one etched side.

For easy handling and in order to fit into the setups for dip-coating and analysis, the wafers were cut into 5 x 10 mm pieces using a diamond cutter. After cutting, the silicon substrates underwent a pre-cleaning procedure of consecutive ultrasonication in purified water, isopropanol and acetone for 30 min each. These steps were repeated three times and finally the silicon substrates were dried with nitrogen.

For comparison two different final cleaning procedures were used:

- The first cleaning procedure involved the use of so called "piranha solution". This is a mixture of 95 % sulphuric acid (H₂SO₄) and 25 % hydrogen peroxide (H₂O₂) in a three to one ration. The silicon substrates were cured in this solution for one hour, thoroughly rinsed with purified water and dried with nitrogen.
- The second cleaning procedure involved successive ultrasonication in isopropanol and acetone for 10 min each. These steps were repeated three times and finally the silicon substrates were dried with nitrogen.

In order to avoid contamination by exposure to air, all final cleaning procedures were performed immediately before further preparation or analysis of the substrates.

2.2 Silanization of silicon substrates

For the silanization of the silicon substrates an APTES solution (99 %) was obtained from Sigma-Aldrich (Saint Louis, United States of America) and diluted with anhydrous toluene (99.9%, max. 0.005 % H₂O) obtained from Merck KGaA (Darmstadt, Germany) to a final concentration of 2 vol%. Both solutions were stored in a glovebox to prevent reaction with water from air.

The cleaned silicon substrates were cured in this solution for either one or two hours, rinsed with toluene and dried with nitrogen. A part of these substrates were additionally ultrasonicated in toluene for 10 min, then rinsed with toluene and dried with nitrogen.

Immediately after preparation the samples were characterized with XPS.

2.3 Preparation of micellar solutions

The micellar solutions were prepared using polystyrene(n)-block-poly-2-vinylpyridine(m) (PS(n)-b-P2VP(m)), n and m representing the number-average molecular weight of each polymer chain (Figure 7).

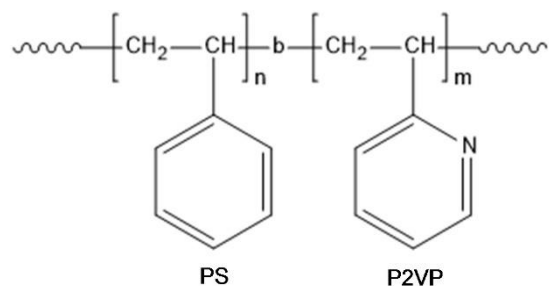


Figure 7: Diblock copolymer polystyrene(*n*)-block-poly-2-vinylpyridine(*m*). With *n* and *m* representing the number of monomer units of each polymer chain.

These diblock copolymers were obtained from Polymer Source Inc. (Dorval, Canada), in various chain length combinations. The number-average molecular weight is calculated as shown in Equation 4 and is a representation of the polymer chain length.

$$M_n = \frac{\sum_i N_i M_i}{\sum_i N_i}$$

Equation 4: Number-average molecular weight (M_n). With N_i the number of polymer molecules of molecular mass M_i .

The various chain length combinations used are summarized in Table 1. Each polymer is assigned a label for ease of reference further on in this thesis and the two most often used polymers (B and H) are highlighted.

Table 1: Overview of the different number-average molecular weight combinations of the polymers used.

Polymer	M_n PS (u)	M_n P2VP (u)
A	248000	195000
B	185000	90000
C	185000	73000
D	175000	70000
E	172000	42000
F	82000	83000
G	50000	16500
H	32500	7800

The first solution (# 794) was prepared by dissolving 25 mg (± 0.2 mg) of diblock co-polymer in 5 ml anhydrous toluene (99.5 %, max. 0.05 % H₂O) obtained from Sigma-Aldrich (Saint Louis, United States

of America). Sigma-Aldrich stopped supplying this product. Unless mentioned otherwise, all other solutions were prepared using anhydrous toluene (99.9%, max. 0.005 % H₂O) bought from Merck KGaA (Darmstadt, Germany)). The solutions were protected from light (to prevent polymer degradation) and stirred for a minimum of three days.

To study how the formation of micelles can be stabilized, some of the solutions were additionally loaded with chloroauric acid (HAuCl₄) in different loading ratios. The chloroauric acid was obtained from Sigma-Aldrich (99.9 %) and stored in a glovebox to prevent hydration.

Some of the solutions received different additives like purified water, methanol, ethanol or combinations of the above. A detailed summary of all micellar solutions, including all additives and analysis methods used, can be found in the supplemental information part one.

Some of the micellar solutions were characterized with DLS to analyse the size and size distribution of the micelles. Information about which samples were characterized in this way can also be found in the supplemental information part one.

2.4 Dip coating

Silicon substrates were dip coated with micellar solutions in order to deposit a hexagonally ordered, dense array of micelles at the substrate surface. For this a home build device was used that consists of an electromagnetic motor connected to a power supply via a three-position switch. This allows to turn the electromagnetic motor in both directions, as well as let it stop in a fixed position. The motor is connected to a gear rack that is mounted to a sample mounting assembly. The speed at which the sample moves in and out of the coating solution can be adapted by changing the voltage of the power supply. The correlation between the applied voltage and the dip coating speed can be found in the supplemental information part two. The dip coating speed can influence the micellar array formation. The higher the dip coating speed, the more micelles are drawn out of the solution resulting in a denser array⁽¹⁰⁾. Figure 8 shows how the micelles are drawn out of the solution to form a monolayer on the substrate during the dip coating process.

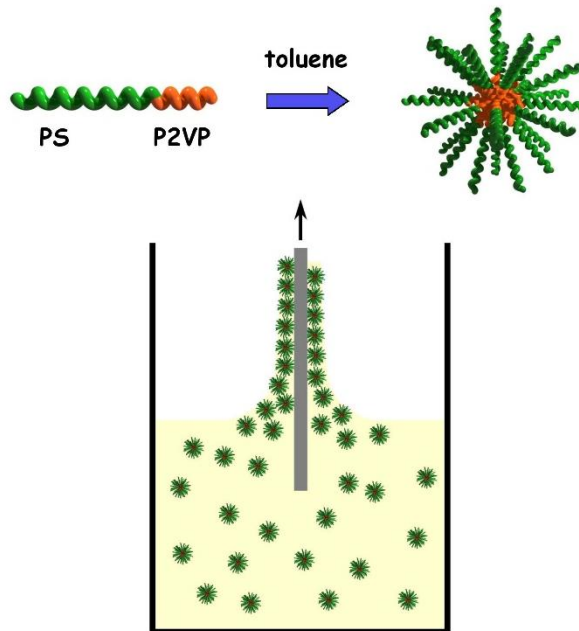


Figure 8: Schematic representation of PS-P2VP micelles and the dip coating process.

After dip coating, the samples were characterized with AFM and XPS. A detailed overview of all dip coated samples and which characterization was performed can be found in the supplemental information part one.

2.5 Oxygen plasma etching

Radio frequency oxygen plasma etching was used to (partially) remove the APTES layer from the silicon substrates. The commercially available plasma etcher was obtained from Plasma Technics Inc. (Racine, United States of America). Unless noted otherwise, the samples were etched at room temperature with 25 W and an oxygen flow rate of 35 sccm.

To estimate the minimum time required to remove the APTES layer completely from the silicon substrate, a batch of silicon substrates was silanized for one hour according to the silanization procedure mentioned in section 2.2. Different substrates of this batch were oxygen plasma etched for 15 s, 30 s, 45 s, 1 min, 2 min and 10 min.

2.6 Nanolithographical patterning of the APTES layer

For nanolithographical patterning of the APTES layer, another batch of silanized substrates was prepared as mentioned above. These samples were dip coated with the micellar solution # 854 and oxygen plasma etched for one minute. After etching, the remaining micelles were removed by repetitive ultrasonication in dimethylformamide (DMF) at 60 °C for one hour.

The samples were imaged with AFM after dip coating, after plasma etching and after the removal of the remaining micelles.

2.7 Hydrogen plasma etching

One bare silicon substrate and one silanized silicon substrate were hydrogen plasma etched to investigate the influence on the wetting behaviour. This was done with a home build plasma etching device at room temperature, 25 W and a pressure of 1×10^{-1} mbar for ten seconds.

2.8 Nanodiamond deposition

Nanodiamond particles of type MSY (0 - 0.05 μm) with D50 of 0.025 μm were obtained from Microdiamant AG (Lengwil, Swiss). This monocrystalline nanodiamond powder, produced by high-pressure, high-temperature synthesis, was treated to contain NV centres. This was done by irradiation with high energy particles followed by thermal annealing ⁽¹¹⁾.

For deposition onto various substrates the nanodiamond powder was dispersed in purified water to a concentration of 1 mg/ml. The dispersion was ultrasonicated for a minimum of three hours prior to use.

The nanodiamond dispersion was used to study the electrostatic adhesion of the nanodiamond particles to different substrates. For this three different samples were prepared; one silicon substrate that was cleaned according to the procedure described in section 2.1, a second silicon substrate was additionally silanized for one hour according to the procedure described in section 2.2 and a third silanized substrate was oxygen plasma etched for one minute according to the procedure described in section 2.5. Immediately after preparation, all substrates were submerged in the nanodiamond dispersion. After one hour the substrates were rinsed with purified water and dried with nitrogen.

2.9 Nanodiamond photoluminescence measurements

In order to investigate the fluorescent properties of the nanodiamond particles after deposition on an APTES coated substrate, photoluminescence measurements were performed. For this a home build confocal setup of the Wide Band Gap Materials group was used. Beside some optics, the most important parts of the setup are the laser, an objective, a monochromator and an avalanche photodiode. The laser of type Gem 532 ($\lambda = 532 \text{ nm}$) was obtained from Laser Quantum GmbH (Konstanz, Germany) and was operated at a power of 1.6 mW. The PLAPON 60XO immerse objective was bought from Olympus and has a numerical aperture of 1.42, a magnitude of 60x. The Cornerstone™ 130 1/8 monochromator (model 74004) was obtained from Newport Spectra-Physics BV (Utrecht, Netherlands). The avalanche photodiode with single photon counting module (SPCM-AQRH-14) was bought from Excelitas Technologies Corp. (Waltham, United States of America). The theoretical spatial resolution of this setup is approximately 300 nm.

In order to fit onto the objective stage of the setup, the samples were mounted on a microscope slide. To protect the samples from the immersion oil used during the measurements, a cover slide was adhered to the sample with a drop of purified water.

Two of the three samples imaged with AFM were used for photoluminescence measurements. The sample with nanodiamonds deposited on a silanized silicon substrate and the sample with nanodiamonds deposited on a silanized silicon substrate that was plasma etched for one minute prior to nanodiamond deposition. First linear scans along the x-axis (width) were obtained at different heights (z-axis) to get a depth profile. Using this depth profile, the precise position of the substrate surface was determined for an x-y-scan (in plane). Additionally a photoluminescence spectrum was obtained at a spot of highest intensity.

3 Results and discussion

3.1 Silicon substrate cleaning procedure optimization

XPS measurements were performed to analyse the effectiveness of the two different cleaning procedures described in section 2.1. The spectrum of a clean silicon substrate should only contain peaks of silicon and oxygen. Additionally a small carbon peak can be expected due to exposure to hydrocarbons in air. Figure 9 shows a survey scan of a silicon substrate that was cleaned using a piranha solution versus a silicon substrate that was cleaned by ultrasonication in isopropanol and acetone. As expected, both spectra show peaks for silicon, oxygen and carbon. The spectrum of the piranha treated substrate indicates the additional presence of nitrogen and sulphur.

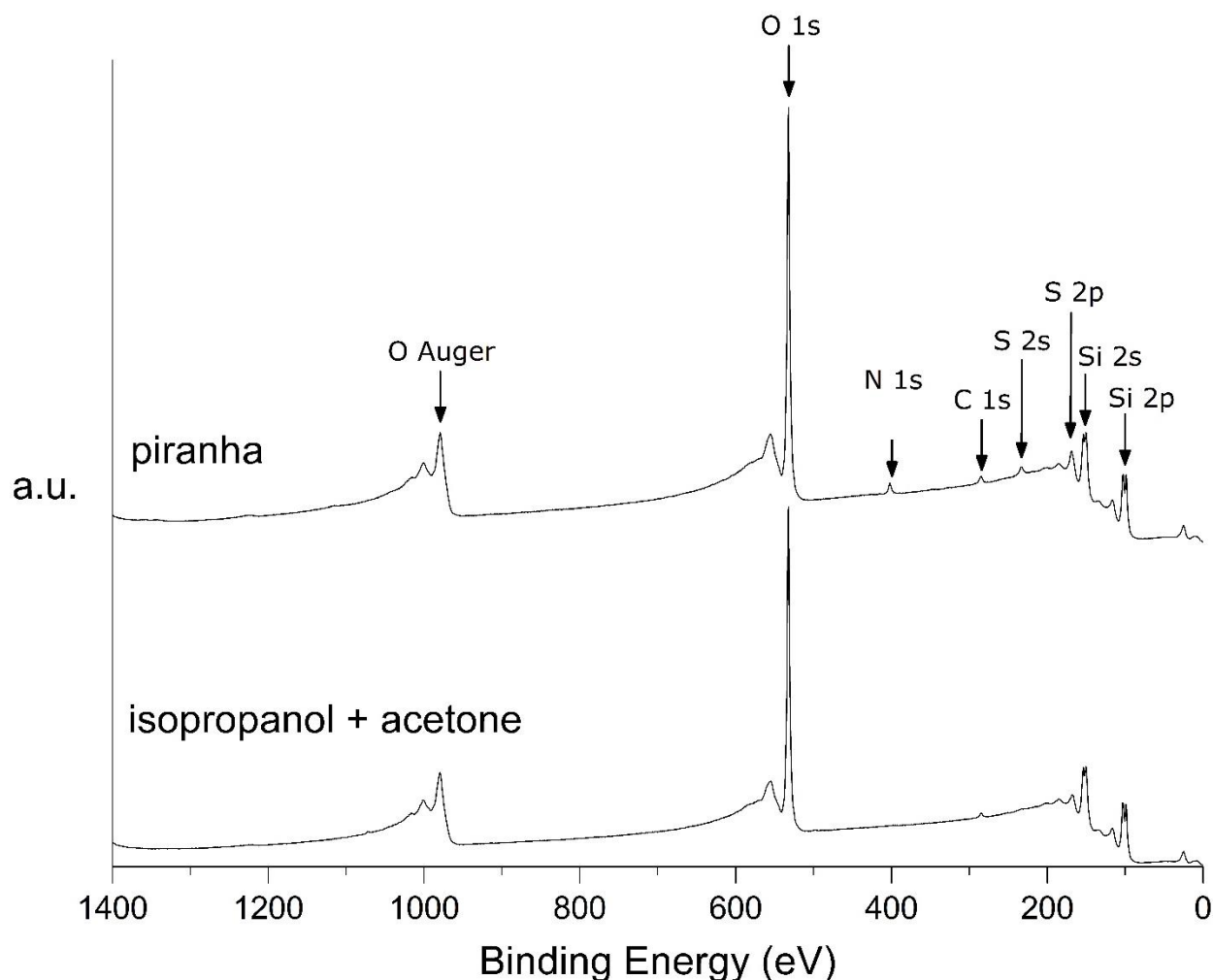


Figure 9: Comparison of different cleaning procedures. XPS survey of piranha treated silicon substrate (top), isopropanol and acetone treated silicon substrate (bottom).

A close-up as shown in Figure 10 confirms the presence of a nitrogen 1s peak at ± 400 eV. The sulphur 2p peak (± 168 eV) and the first plasmon of the silicon 2s peak overlap, but the sulphur 2s peak at ± 232 eV

shows the presence of a sulphur contamination. The relative height of the carbon 1s peak of the piranha treated substrate is higher as compared to the substrate ultrasonicated in isopropanol and acetone, indicating additional carbon contaminations besides nitrogen and sulphur.

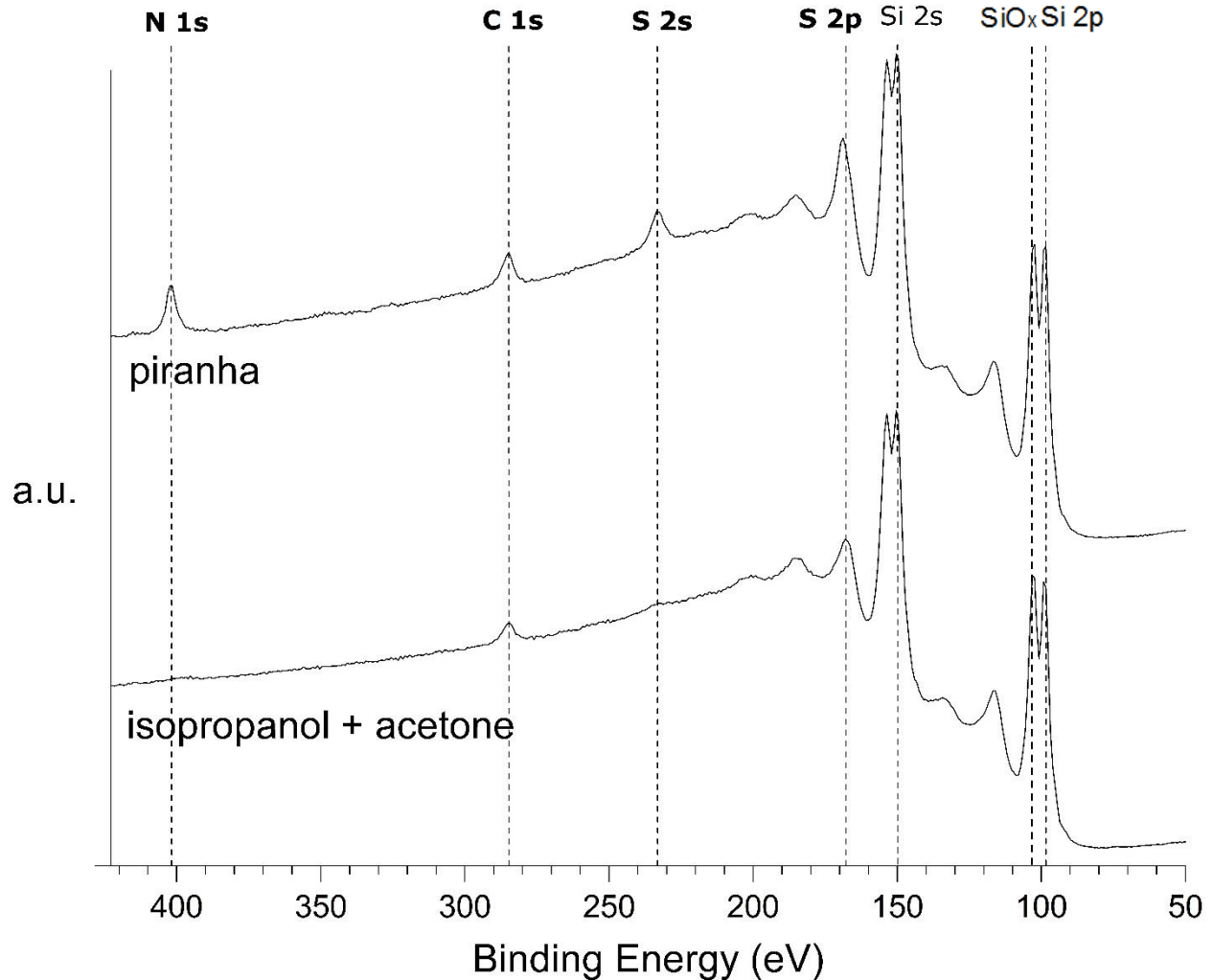


Figure 10: Comparison of different cleaning procedures. XPS close-up of piranha treated silicon substrate (top), isopropanol and acetone treated silicon substrate (bottom).

Because of the contaminations (sulphur, nitrogen and carbon) introduced during the piranha treatment, all further mentioned substrates were cleaned by ultrasonication in isopropanol and acetone according to the cleaning procedure mentioned in section 2.1.

Especially the absence of any nitrogen contaminations is of crucial importance for the correct approximation of the APTES layer thickness later on in this thesis. Because this enables the use of nitrogen as a fingerprint for the APTES layer.

3.2 Silanization of silicon substrates

Formation of a thin and homogeneous APTES layer is the foundation and the first step of the five step technique presented in this thesis. To study the best conditions for the formation of an optimal APTES layer, a series of different experiments was conducted.

The APTES molecules contain a silicate group which enables an estimation of the APTES layer thickness with Equation 5. This equation derives the layer thickness by using the attenuation length of the silicon 2p photoelectrons in silicon oxide, the photoelectron take-off angle, the ratio of silicon 2p intensities of "infinitely thick" (> 30 nm) silicon and silicon oxide and the ratios of the intensities of the silicon and silicon oxide peaks of the sample.

$$d_{ox} = \lambda_{ox} \sin \theta \ln \left(\frac{I_{ox}}{\beta I_{Si}} + 1 \right)$$

Equation 5: Silicon oxide layer thickness calculation. Where d_{ox} is the thickness of the silicon oxide layer, λ_{ox} is the attenuation length of the silicon 2p photoelectrons in silicon oxide, θ is the photoelectron take-off angle (the angle between the sample surface and the incident beam), β is the ratio of the intensities of "infinitely thick" silicon oxide and silicon respectively and I_{ox}/I_{Si} is the ratio of the intensities measured.

In literature values for λ_{ox} ranging from 2.4 – 3.8 nm and for β from 0.6 – 1.01 are reported⁽¹²⁻¹⁶⁾. For all calculations mentioned in this thesis the values 2.7 nm for λ_{ox} and 0.8 for β were used. OriginPro 9 software was used to integrate the silicon and silicon oxide peaks in order to determine the peak intensities.

3.2.1 Influence of ultrasonication on APTES layer thickness

In order to investigate the influence of ultrasonication on the APTES layer thickness, two silanized samples of the same batch are compared. The first sample was measured with XPS immediately after silanization. The second sample was additionally ultrasonicated in toluene for ten minutes prior to measurement. All following XPS spectra have been normalized for the silicon 2p peak for ease of comparison.

Nitrogen and carbon are exclusively present in the APTES layer due to the optimized cleaning procedure mentioned above. The nitrogen 1s and the carbon 1s peaks indicate the presence of APTES on both samples (Figure 11). However, after ultrasonication the nitrogen 1s and carbon 1s peaks are significantly reduced. This indicates that the total APTES layer thickness is reduced.

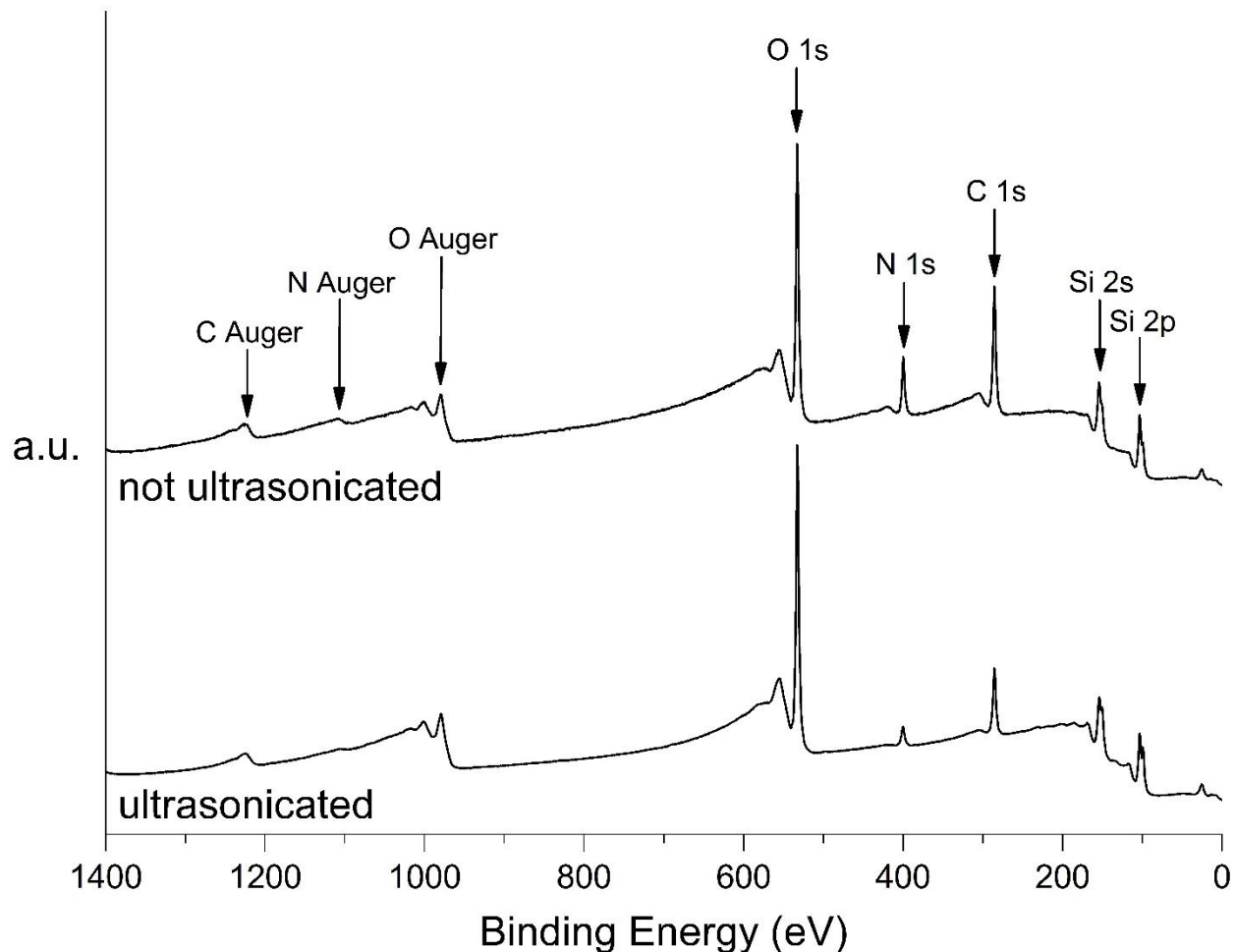


Figure 11: Effect of ultrasonication on the APTES layer thickness. XPS survey spectra of silanized silicon substrates (2 h), with (bottom) and without additional ultrasonication for 10 min in toluene (top).

A high resolution XPS spectrum of the silicon 2p region is used to estimate the thickness of the APTES layer of both samples (Figure 12).

The silicon oxide peak of the spectra includes photoelectrons coming from the APTES layer and photoelectrons coming from the underlying silicon oxide layer. In order to correct for the thickness of the native silicon oxide layer, a silicon substrate (of the same batch that was used for silanization) was analysed. Using Equation 5 the estimated silicon oxide layer thickness of this reference sample is calculated to be 2.16 nm. All APTES layer thicknesses mentioned further in this thesis have been corrected for this value and reflect just the thickness of the APTES layer itself.

Comparison of the APTES layer thicknesses before and after ultrasonication shows that the layer is reduced by 60 % after ten minutes of ultrasonication in toluene.

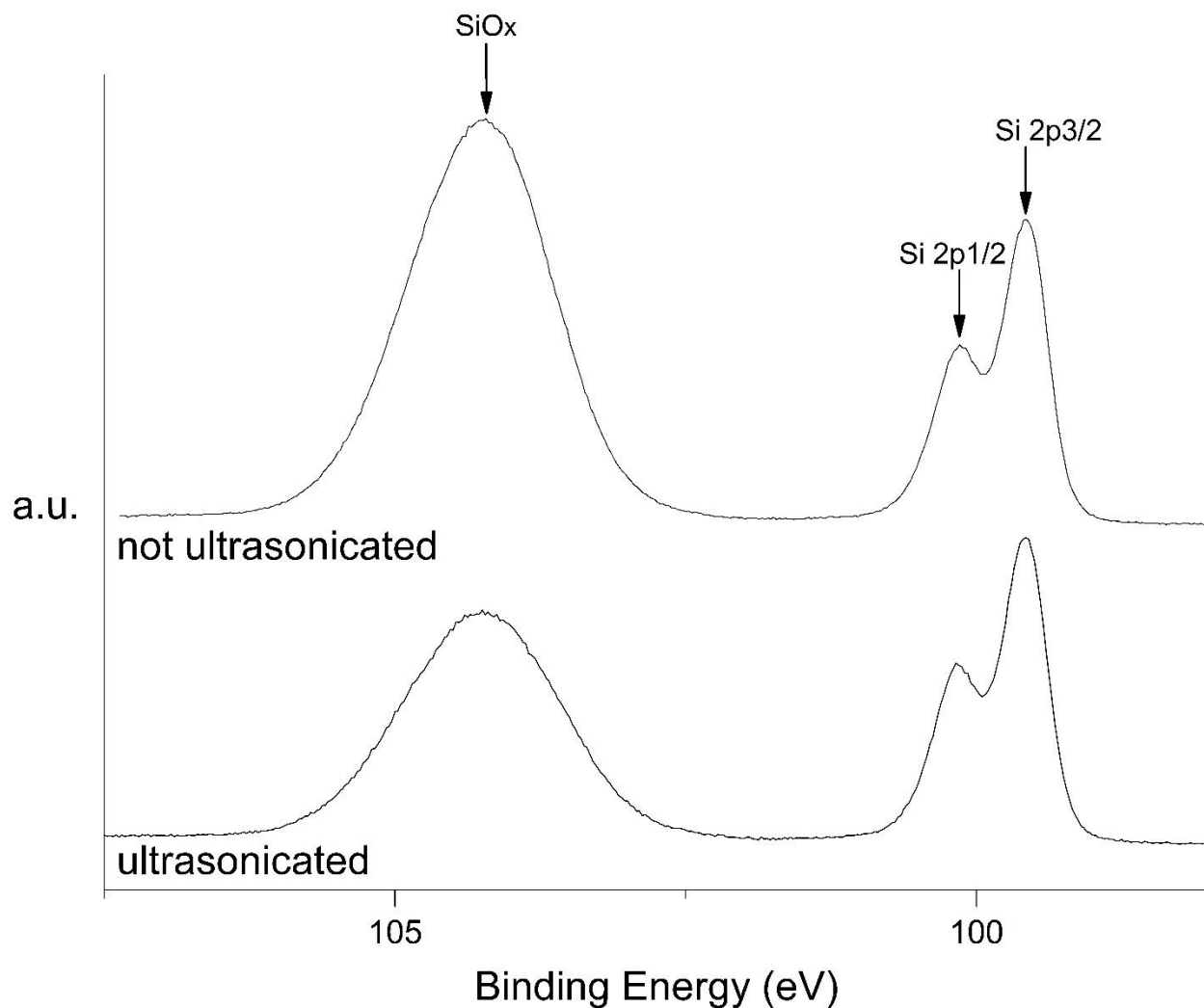


Figure 12: Comparison of the silicon to silicon oxide ratio. High resolution XPS spectra of a silanized silicon substrate (top) and a silanized silicon substrate that was ultrasonicated in toluene for 10 min (bottom).

3.2.2 Influence of curing time on APTES layer thickness

To study the influence of the curing time on the thickness of the APTES layer, two freshly cleaned silicon substrates were silanized simultaneously. The first sample was removed from the APTES solution after one hour, the other sample was removed after two hours. Thereafter both samples were ultrasonicated in toluene for 20 min and analysed with XPS. The high resolution spectra of the silicon 2p region used for integration and calculation of the layer thickness are shown in Figure 13. The estimated APTES layer thicknesses are calculated to be 1.22 nm and 4.45 nm for the one and two hour cured sample respectively. This is a reduction of 73 % by reducing the curing time by one hour.

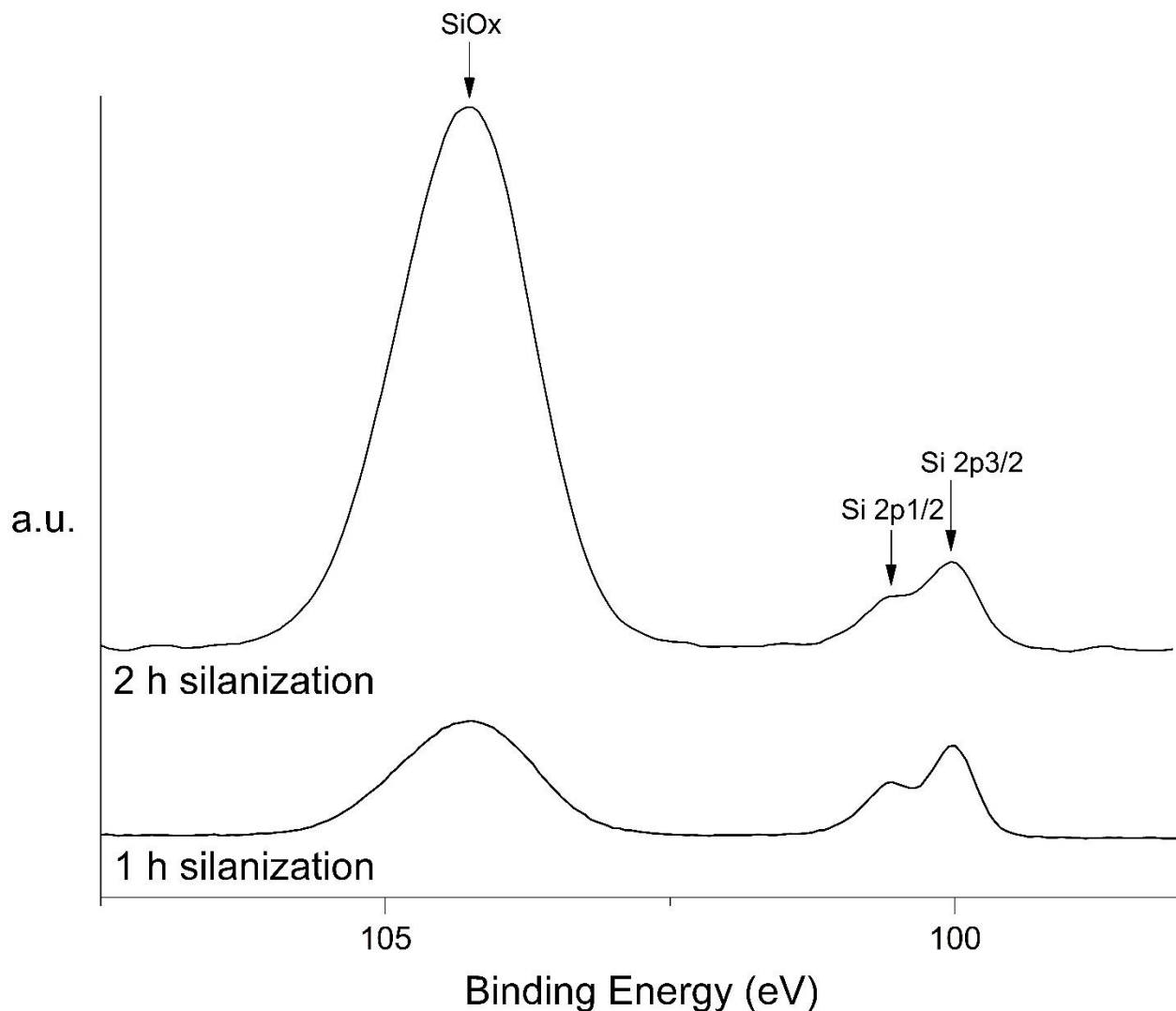


Figure 13: Comparison of the silicon to silicon oxide ratio. High resolution XPS spectra of a silicon substrate silanized for two hours (top) and one hour (bottom) both samples were ultrasonicated in toluene for 20 min after silanization.

3.2.3 Oxygen plasma etching conditions for APTES removal

To determine the minimum etching time required to remove the APTES layer, a batch of silicon substrates, silanized for one hour and ultrasonicated for 20 min, was plasma etched for increasing exposure times. By analysis of the high resolution XPS spectra of the silicon 2p region, no direct correlation between the etching time and the silicon to silicon oxide ratio can be found (Figure 14).

This can be the result of how the experiment was conducted. The time available during this master thesis was limited. Therefore a batch of identical silanized samples, sequentially etched for increasing time, was used to simultaneously be loaded and measured with XPS. A consequence of this is that the overall temperature in the plasma chamber might have increased between the different samples. This might have induced differences in the oxidation of the native silicon oxide layer during the oxygen plasma treatment, adding an additional variable to the system, making it very complex to study.

Therefore the calculated total silicon oxide layer thicknesses cannot be corrected for the native silicon oxide layer thickness and no conclusions can be drawn from comparison of the total silicon oxide layer thicknesses.

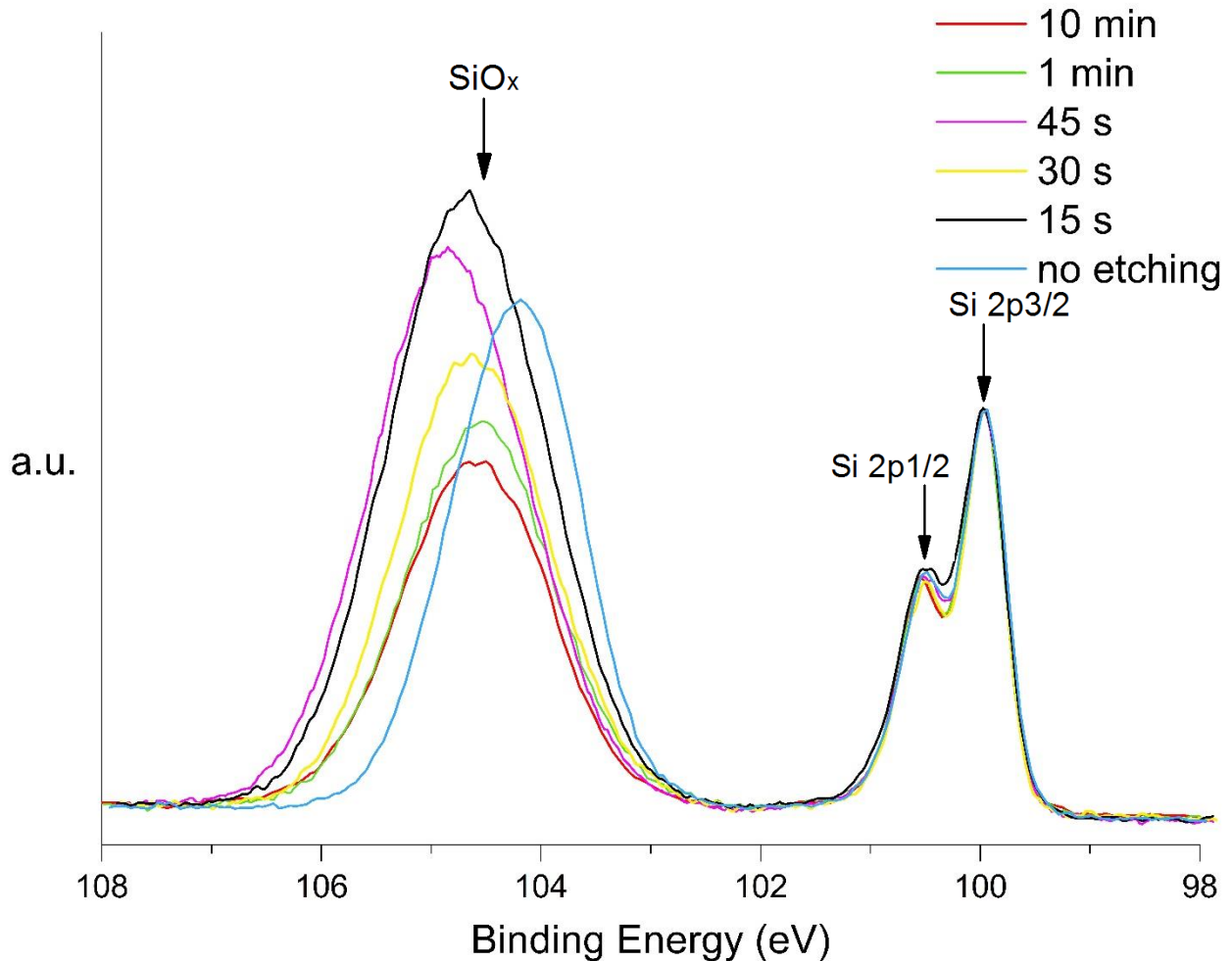


Figure 14: Comparison of the silicon to silicon oxide ratio. High resolution XPS spectra of the silicon 2p region. Silicon substrates silanized and ultrasonicated in toluene for 20 min in one batch and exposed to oxygen plasma for increasing times.

However, a rough approximation of the APTES layer thickness can be calculated by using the high resolution XPS spectra of the nitrogen 1s region (Figure 15). For this the decrease in APTES layer thickness is presumed to be directly correlated with the decrease in nitrogen 1s signal intensity. The absolute APTES layer thickness of the unetched sample is known to be 1.22 nm and can be used as a reference. The APTES layer thicknesses of the etched samples are calculated by multiplying the known height of the unetched sample with the ratios of the nitrogen 1s peak intensity of each etched sample over the nitrogen 1s peak intensity of the reference sample. The result of APTES layer approximation can be found in Figure 16.

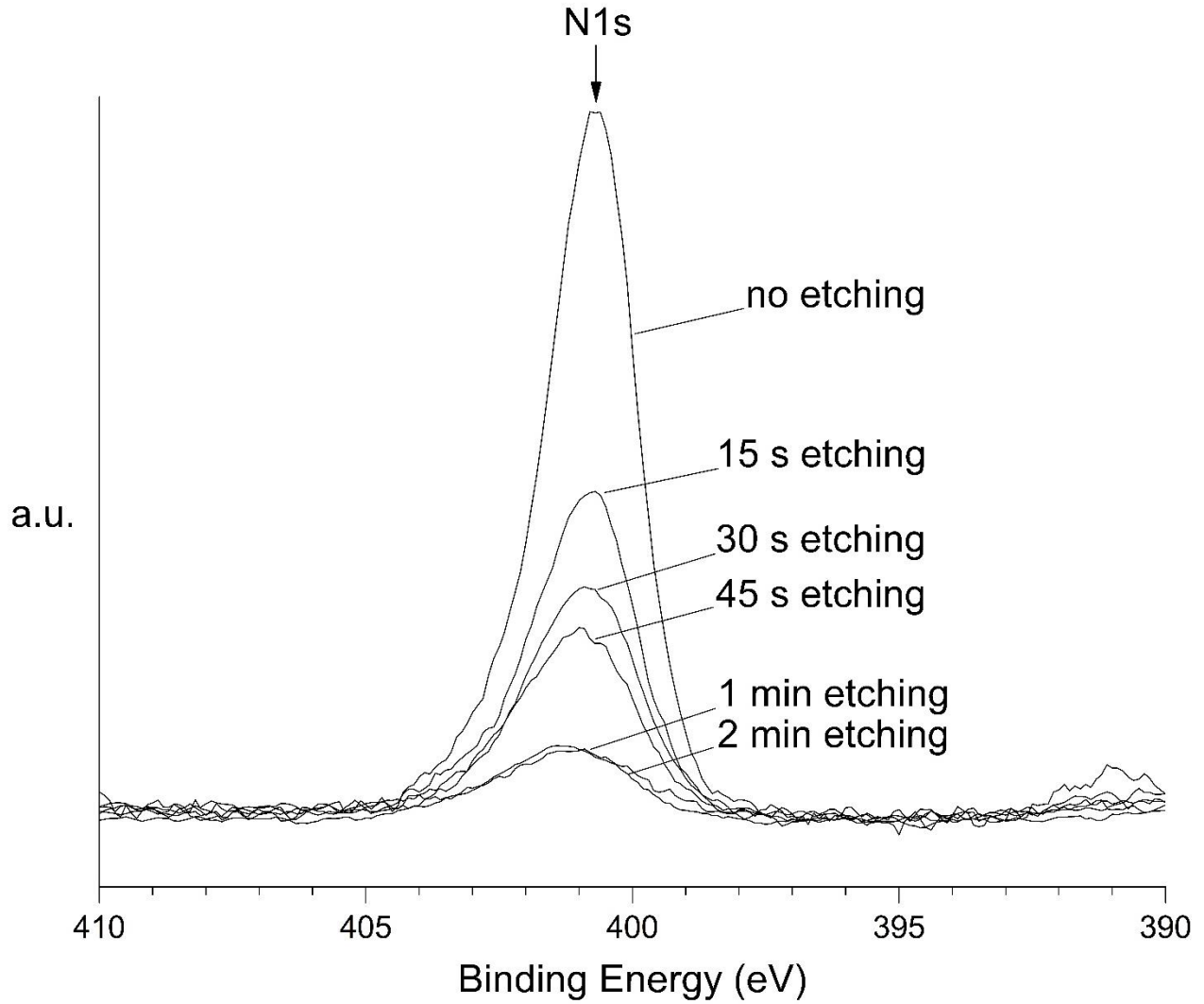


Figure 15: Influence of increasing etching time on the APTES layer thickness. High resolution XPS spectra of the nitrogen 1s region of salinized silicon substrates that were plasma etched for increasing times.

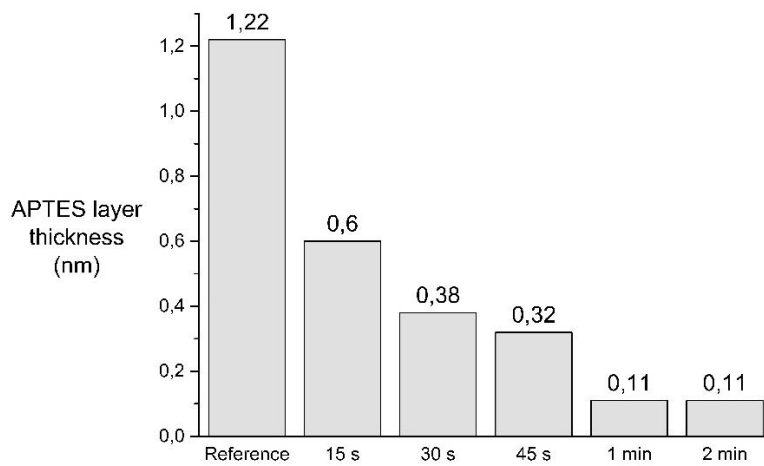


Figure 16: Approximation of the APTES layer thickness after increasing etching times.

3.3 Optimization of the micelle formation for use as etch mask

A micellar solution was prepared for dip coating and subsequent imaging with AFM to analyse the dimensions of the array. This was done by dissolving 24.90 mg of polymer B in 5 ml toluene. After five days of stirring the solution was dip coated onto a silicon substrate and a silanized silicon substrate (Figure 17).

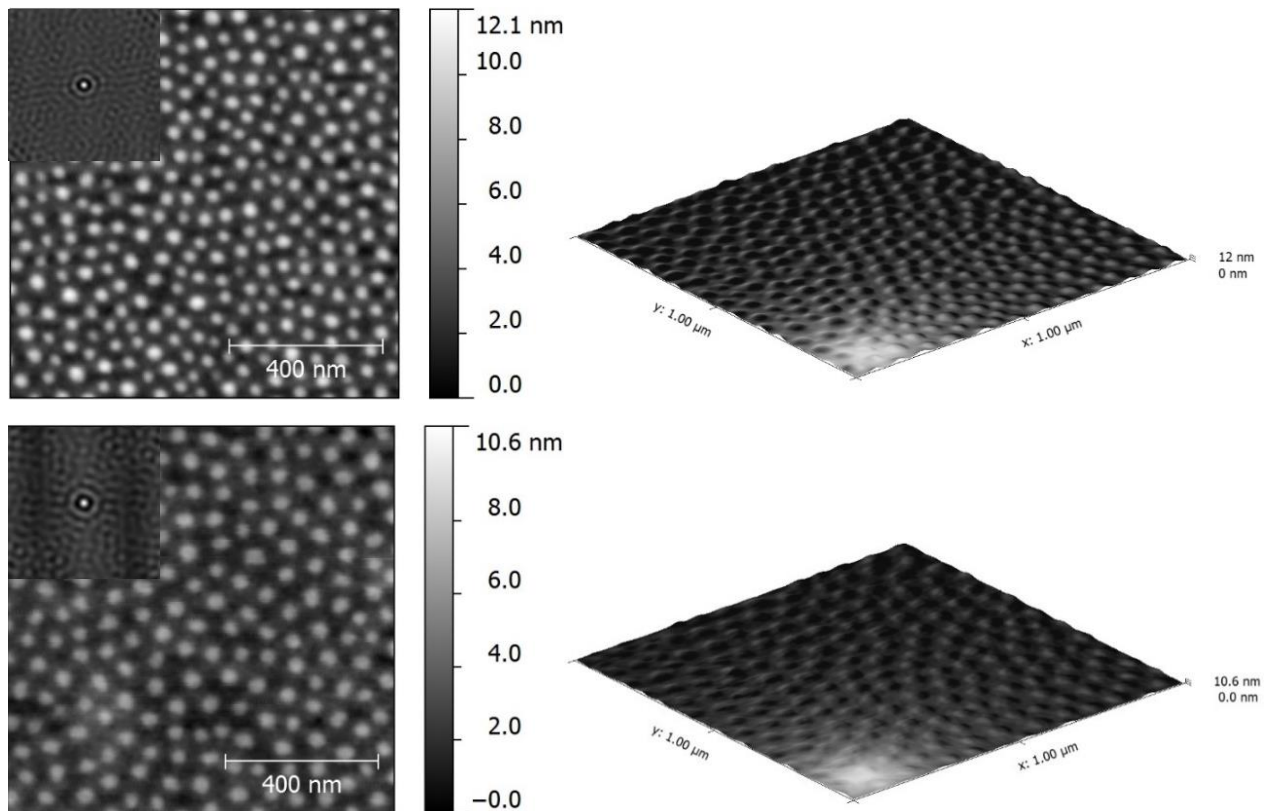


Figure 17: AFM image of micellar solution # 794 dip coated on a silicon substrate (top) and on a silanized silicon substrate (bottom).

To analyse the dimensions in more detail Gwyddion software was used to determine the micellar diameter and to create a line profile of both samples (Figure 18).

Both samples show a similar array quality with indications for hexagonal short range order, but the micelles on the silanized substrate are slightly reduced in height accompanied by a larger inter micellar distance. This might be a consequence of the positive charge of the APTES layer.

The height of the micelles on the silicon substrate and the silanized silicon substrate are respectively about 8 and 6 nm, the diameter is about 30 and 34 nm and the inter micellar distance is about 70 and 80 nm. These are etch mask dimensions suitable for the deposition of the fluorescent nanodiamonds.

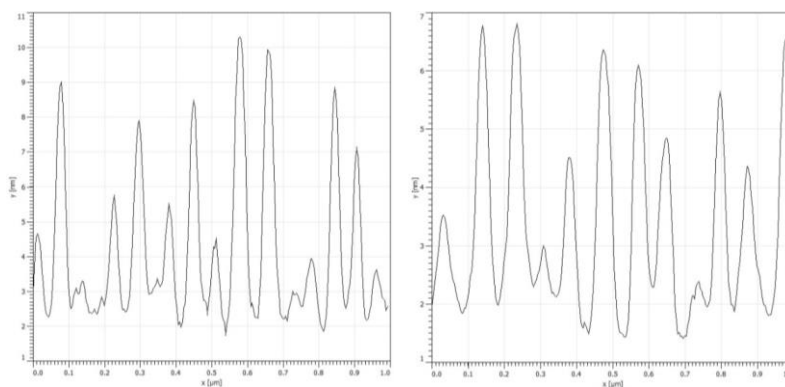


Figure 18: Line profiles of micellar solution # 794 dip coated on a silicon substrate (left) and on a silanized silicon substrate (right).

After the successful preparation of micellar solution # 794, the formation of micelles could not be repeated any more afterwards. With AFM images similar to the one shown in Figure 19. The silicon substrates are covered by polymer aggregates, no micelle like structures are found.

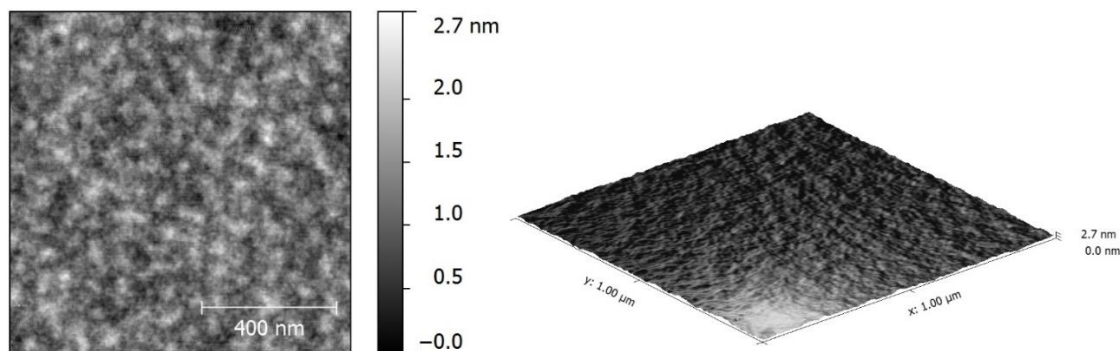


Figure 19: AFM image of micellar solution # 802 dip coated onto a silicon substrate.

At first an unknown contamination was suspected to be the cause of the problem. In order to investigate this suspicion, all possible sources of contamination were systematically excluded. All the glassware and instrumentation was thoroughly cleaned or replaced, a new bottle of solvent was used, different polymers were used but the problem remained.

After ruling out any contamination as cause of the problem, other ways to stabilise the micelle formation were investigated.

Solution # 839 was stabilised by addition of chloroauric acid in a loading ratio of 0.5. As can be seen in Figure 20, this approach stabilised the micelle formation, resulting in a wide array with an inter micellar distance of approximately 110 nm. The micelles have a diameter of about 36 nm and a height of about 25 nm.

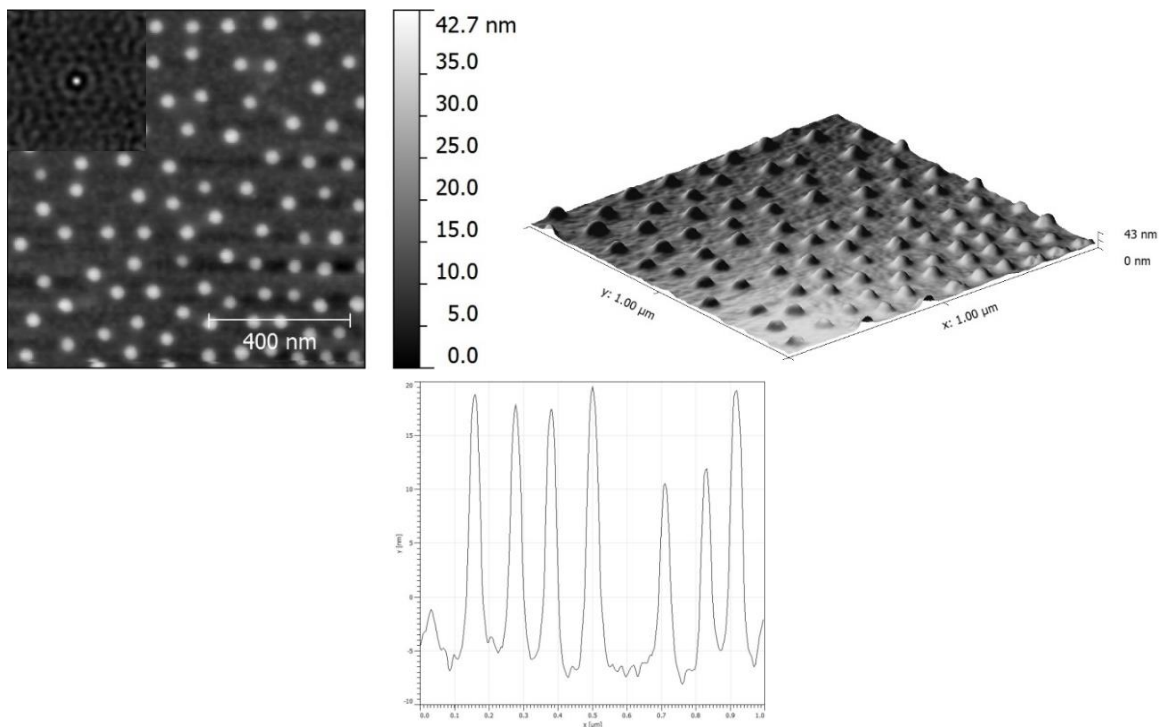


Figure 20: AFM image and line profile of micellar solution # 839 dip coated onto a silicon substrate.

While addition of chloroauric acid stabilises the micelle formation, it hinders the removal of the micelles from the substrate. Because the micelles must be removed prior to the deposition of the nanodiamond particles, stabilising the micelle formation with chloroauric acid is not an option.

Therefore alternative ways for the formation of micelles were investigated. Addition of different amounts of methanol (50 – 500 μl) to the standard protocol turned out to be unsuccessful.

Another approach was to ultrasonicate the solutions for one hour with purified water and methanol as additives. The solutions with a ratio of 150 μl methanol to 50 μl purified water as additives (# 842 and # 843) showed promising DLS results with sizes of 45 to 48 nm at count rates of over 400 kcps. However, AFM images of silicon substrates dip coated with these solutions indicated wetting problems (Figure 21).

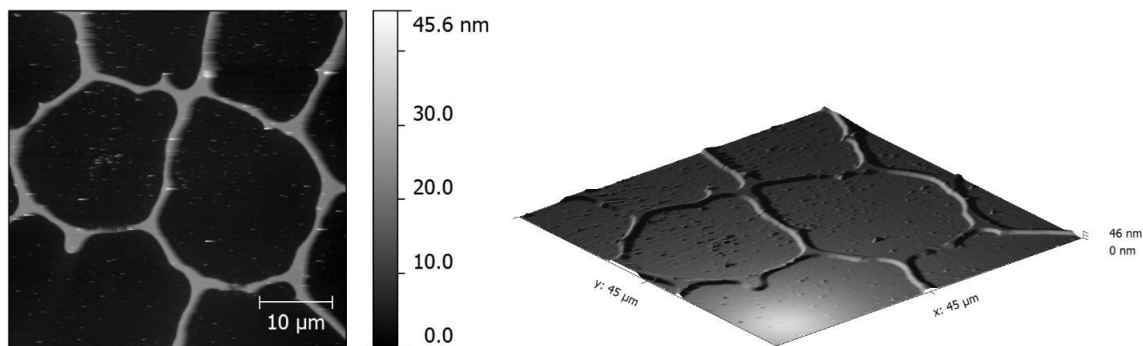


Figure 21: AFM image of micellar solution # 843 dip coated onto a silicon substrate indicates a wetting problem.

3.4 Wetting behaviour of APTES and silicon oxide

Because of the array formation issues caused by wetting problems, the wetting behaviour of APTES and silicon oxide was investigated with contact angle measurements.

For this several silicon substrates and silanized silicon substrates were either exposed to air for several days, ultrasonicated in toluene for 20 min, oxygen plasma etched for one minute or hydrogen plasma etched for one minute.

Ultrasonication was performed to ensure that all hydrocarbons and other contaminations coming from air are removed. The plasma etching conditions were chosen so that the surfaces are functionalised without completely removing the APTES and the silicon oxide layers.

Multiple contact angle measurements were performed for each sample. The average contact angles are summarized in Table 2.

Table 2: Contact angles of APTES and silicon after different treatments.

Treatment	APTES	Silicon
Air exposure	71 °	46 °
Ultrasonication	60 °	42 °
Oxygen plasma etching	< 5 °	< 5 °
Hydrogen plasma etching	42 °	23 °

All samples show a high wettability (contact angle < 90 °). Overall the silicon substrates are more hydrophilic than the APTES coated substrates.

The samples exposed to air have the lowest wettability due to hydrocarbons deposited from air. Those hydrocarbons are removed by ultrasonication which results in an increase of wettability.

Exposure to oxygen plasma makes both surfaces super hydrophilic (contact angle ~ 0 °). This is to be expected due to the induced oxygen termination and increased surface roughness.

Hydrogen plasma etching however did not increase the hydrophobicity, as was expected. The etching conditions may have been too mild to induce sufficient hydrogen containing groups at the surface. The observed increase in wettability can be explained by the removal of hydrocarbons (similar as with the ultrasonication) and by the increased roughness of the surface (similar to the oxygen plasma treatment).

Overall the wetting behaviour of silicon and APTES is very similar. Once the micelle formation works, the deposition on APTES coated substrates should work as good as on silicon (Figure 17).

3.5 Nanodiamond deposition on APTES and silicon oxide

Negative charged nanodiamond particles can electrostatically bind to a positively charged APTES layer, while being repelled by a silicon oxide layer that has a negative charge.

In order to prove this, three different samples were submerged in a nanodiamond dispersion under identical conditions. The first sample was a silicon substrate that was cleaned according to the cleaning procedure described in section 2.1. The second and third sample were additionally functionalized with an APTES layer according to the procedure described in section 2.2. Finally the third sample was plasma etched for one minute as described in section 2.5.

AFM images indicate the presence of a nanodiamond particle layer on top of the APTES functionalized substrate while there is no sign of nanodiamond particles on the silicon oxide substrate. On the third sample, only some isolated particles are present.

AFM images with a maximum scan size of 10 x 10 μm were obtained at multiple positions on all samples. A representative image of each sample is shown in Figure 22. Images with a scan size of 5 x 5 μm are chosen to ensure that the particle height is still visible on the presented scale.

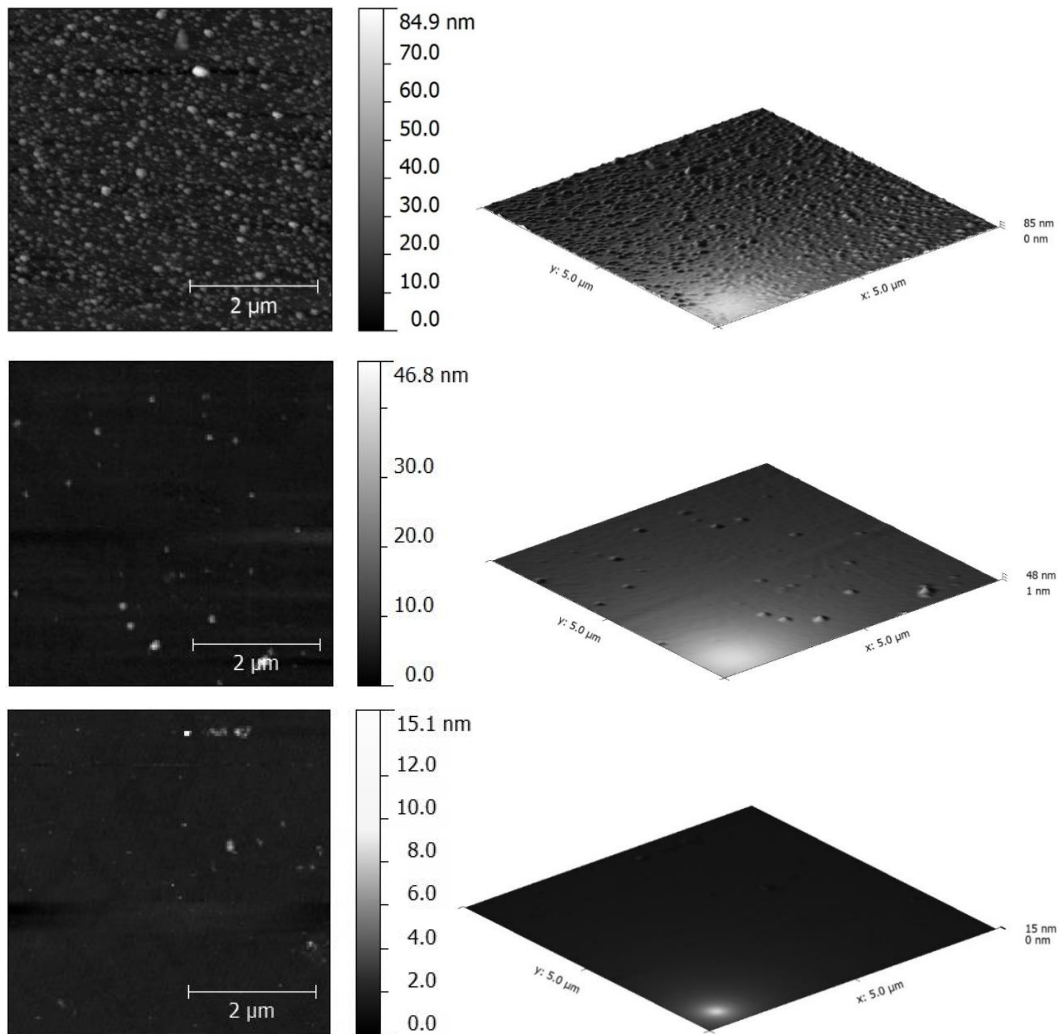


Figure 22: AFM images of nanodiamond deposition on APTES (top), APTES removed by oxygen plasma etching (middle) and silicon oxide (bottom).

The AFM images of the nanodiamond particles deposited on the APTES functionalized substrate show particle like structures with an average height of 20-30 nm and exceptional structures of up to ± 90 nm. This corresponds with the size distribution specified by the supplier of the nanodiamond particles.

XPS spectra were obtained to confirm that the structures seen on the AFM images are nanodiamond particles. The XPS survey spectra shown in Figure 23 display a significant increase of the carbon 1s signal and a decrease of the nitrogen 1s, silicon 2s and silicon 2p signal. This confirms that the particles imaged with AFM are nanodiamonds.

The nanodiamonds almost exclusively exist out of carbon that gives rise to the increased carbon 1s signal and the nitrogen 1s, silicon 2s and silicon 2p signals are damped by the nanodiamond particles. However, the fact that these signals are still present, indicates that the nanodiamond layer is not homogeneously covering the whole surface. Otherwise the photoelectrons emitted by the underlying silanized silicon substrate would not be able to reach the surface of the sample.

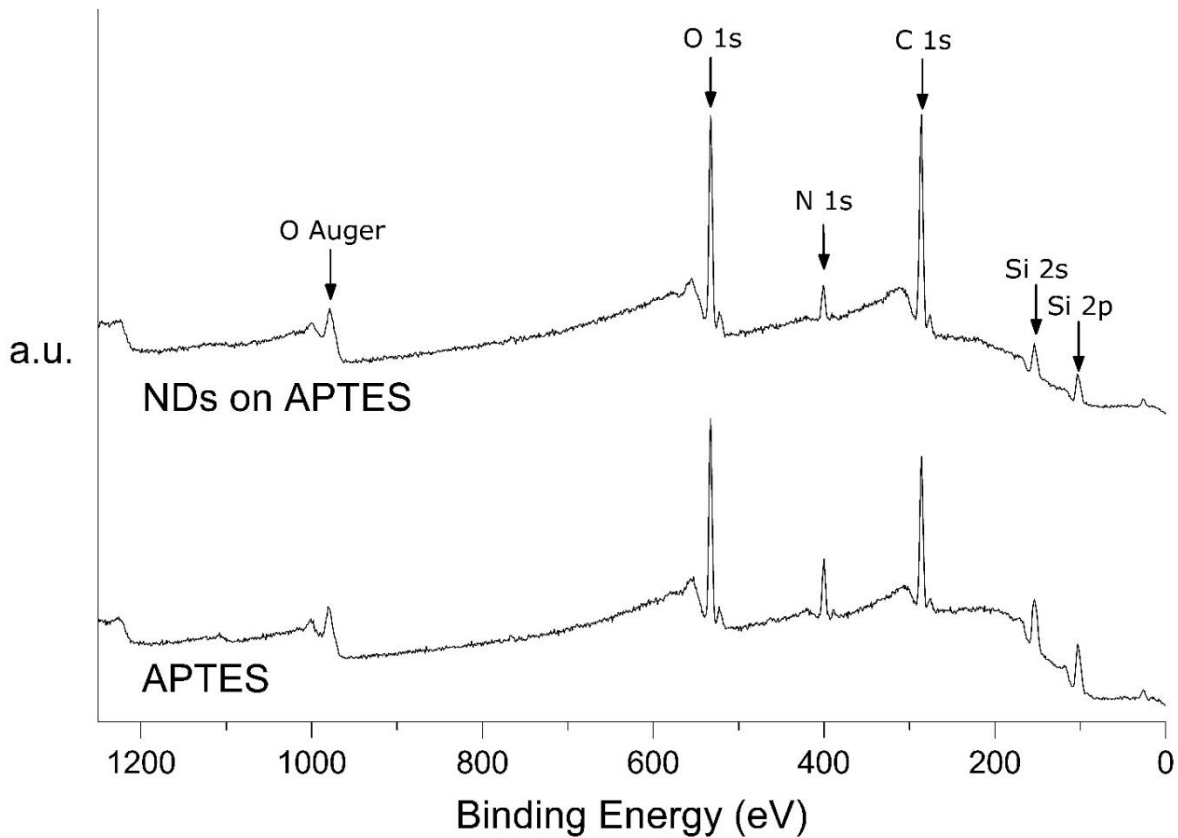


Figure 23: XPS survey spectra of a silanized silicon substrate with (top) and without nanodiamonds deposited (bottom).

3.6 Analysis of the nanodiamond photoluminescence

The above mentioned nanodiamond particles deposited on a silanized silicon substrate were analysed with a confocal setup in order to investigate the photoluminescent properties.

Figure 24 shows a bright fluorescent signal (millions of counts) over the entire scan area of $10 \times 10 \mu\text{m}$ for the nanodiamonds deposited on a silanized silicon substrate (left).

In contrast for the nanodiamonds deposited on the plasma etched silanized silicon substrate, only a single bright spot (hundred thousands of counts) is found on a scan area of $20 \times 20 \mu\text{m}$. The less bright spots (ten thousands of counts) on the scan area are not deriving from NV centres of the nanodiamonds. This was proven by focusing the laser on the spots and following the evolution of the intensity over time. A decrease in intensity was seen due to photo bleaching. NV centres are not prone to photo bleaching, hence the spots are no NV centres.

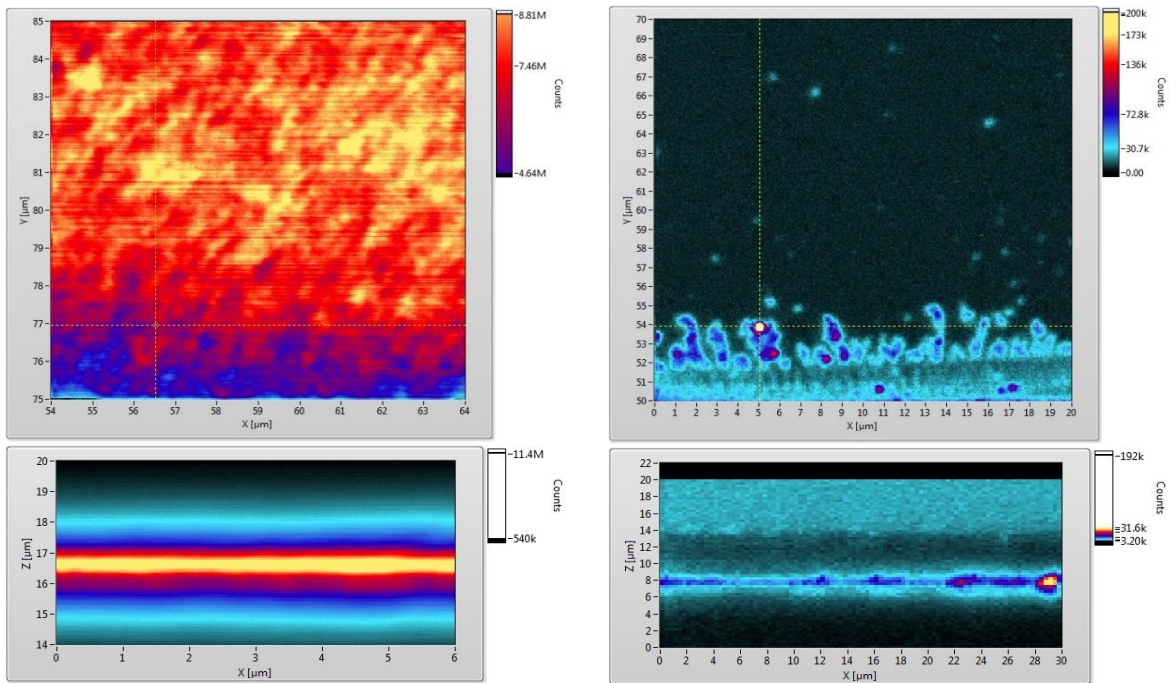


Figure 24: Confocal photoluminescence images of nanodiamond. Nanodiamond on silanized silicon oxide prior to plasma etching (left) and after plasma etching (right). On top are the x-y scan images and on the bottom are the depth profiles.

A photoluminescence spectrum was obtained to confirm the presence of the NV^0 and NV^- centres, characteristic for the nanodiamond particles used. The spectrum shows the typical zero-phonon lines (ZPL) of the NV^0 centre at 575 nm and 640 nm for the NV^- centre (Figure 25).

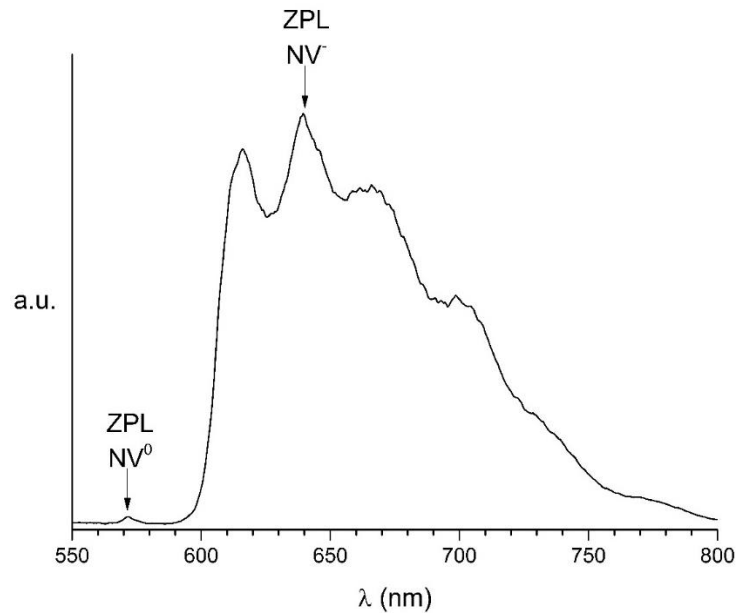


Figure 25: Photoluminescence spectrum of the nanodiamond particles. With the zero-phonon line (ZPL) of the NV^0 at 575 nm and the ZPL of the NV^- at 640 nm.

4 Conclusion and future prospects

At the end of this master thesis it can be concluded that fundamental steps towards the development of nanoscaled arrays of highly fluorescent nanodiamonds have been taken.

With respect to the optimisation of the silicon substrate cleaning procedure, it can be concluded that the piranha cleaning procedure involves the use of hazardous chemicals, is more time consuming and induces contaminations. Therefore, cleaning the silicon substrates by sequential ultrasonication in acetone and isopropanol is the preferred cleaning method.

The optimum conditions for silanization are curing the freshly cleaned silicon substrates for one hour in a 2 vol% APTES solution followed by ultrasonication in toluene for 20 min. In this way the formation of a thin (1.22 nm) and homogenous APTES layer has been achieved.

It was not possible to estimate the APTES layer thickness after different etching times by using the silicon to silicon oxide ratio. This was the consequence of the experimental setup. In order to reduce the time required for the experiment, a batch of multiple samples was prepared and analysed simultaneously, adding an additional variable to the system and resulting in difficulties with the layer thickness estimation. This demonstrates how complex surface science is and that small changes can have a large influence. In the future this experiment should be repeated, but by using the same sample and sequentially exposing it to oxygen plasma and analysing the silicon 2p region with XPS.

However, the approximated APTES layer thickness after different etching times was calculated by using the nitrogen 1s peak. After one minute of plasma etching the APTES layer thickness was reduced to a minimum. Increasing the etching time any further had no additional effect on the nitrogen 1s peak intensity. It can be assumed that the APTES layer is completely removed after exposure to oxygen plasma for one minute.

It has been proven that it is possible to completely remove the APTES layer by exposure to oxygen plasma for one minute. This is an important aspect of the used approach. The APTES layer needs to be completely removed in between the micellar etch mask before the mask is etched away itself. Otherwise no clear pattern can be achieved.

Regarding the micellar approach it can be concluded that it involves a delicate balanced system that can easily be disturbed by small changes. After switching to toluene from another supplier, it was not possible to form micelles according to the standard protocol. The cause of this problem is still uncertain but it is suspected that the original toluene had minor impurities which stabilised the micelle formation.

While it was possible to stabilise the micelle formation by addition of chloroauric acid, this impedes the removal of the micelles after the plasma etching step. DLS confirmed the formation of micelles by using purified water and methanol as additives and ultrasonication of the micelle solution for one hour. However these solutions showed wetting problems after dip coating. In the future it should be tried to create micelles by the core-stabilised micellar approach.

Regarding the deposition of the micelles onto the substrates can be concluded that the wettability of the substrates is improved by exposure to air. Resulting in better arrays which can further be fine-tuned by adapting the dip coating speed. The faster the dip coating speed, the denser the array.

Furthermore it has been demonstrated that the negatively charged fluorescent nanodiamond particles electrostatically bind to the positively charged APTES layer, while being repelled by the silicon substrates. It has also been proven that the highly fluorescent NV centres in the nanodiamond particles keep their photoluminescent properties after deposition.

The final conclusion of this master thesis is that the novel technique developed by Li Wang et al. ⁽¹⁾ can be adapted for the formation of nanoscaled arrays of highly fluorescent nanodiamond particles. It has been demonstrated that all components of the technique function separately. Once the problem regarding the micellar approach has been tackled, all pieces of the puzzle should come together to form the first major breakthrough in the development of fluorescent nanodiamond based (bio)sensors.

References

1. Wang L, Montagne F, Heinzelmann H, Pugin R. Electrostatic-guided positioning of gold colloids using periodic nanopatterns produced by block copolymer lithography. *Journal of Materials Chemistry*. 2011;21(6):1689-92.
2. Qin W, Ding D, Liu J, Yuan WZ, Hu Y, Liu B, et al. Bioimaging: Biocompatible Nanoparticles with Aggregation-Induced Emission Characteristics as Far-Red/Near-Infrared Fluorescent Bioprobes for in Vitro and In Vivo Imaging Applications (*Adv. Funct. Mater.* 4/2012). *Advanced Functional Materials*. 2012;22(4):665.
3. Grotz B, Hauf MV, Dankerl M, Naydenov B, Pezzagna S, Meijer J, et al. Charge state manipulation of qubits in diamond. *Nature Communications*. 2012.
4. Attension. Critical Micelle Concentration. 2009. Available from: <http://www.attension.com/critical-micelle-concentration.aspx>.
5. Briggs D, Seah MP. *Practical Surface Analysis Second Edition*: Wiley; 1996.
6. Moulder JF, Stickle WF, Sobol PE, Bomben KD. *Handbook of X-ray Photoelectron Spectroscopy*. Japan: ULVAC-PHI Inc.; 1995.
7. Meyer E, Wiesendanger R, Morita S. *Noncontact atomic force microscopy*: Berlin Springer; 2002.
8. SecretDisc. AFM (used) cantilever in Scanning Electron Microscope, magnification 1000x 2008. Available from: [http://commons.wikimedia.org/wiki/File:AFM_\(used\)_cantilever_in_Scanning_Electron_Microscope,_magnification_1000x.GIF](http://commons.wikimedia.org/wiki/File:AFM_(used)_cantilever_in_Scanning_Electron_Microscope,_magnification_1000x.GIF).
9. LSInstruments. *Dynamic Light Scattering: Measuring the Particle Size Distribution* 2014. Available from: http://www.lsinstruments.ch/technology/dynamic_light_scattering_dls/.
10. Schwartz L, White L. *Modelling of the dip-coating process*. 1994.
11. Havlik J, Petrakova V, Rehor I, Petrak V, Gulka M, Stursa J, et al. Boosting nanodiamond fluorescence: towards development of brighter probes. *Nanoscale*. 2013;5(8):3208-11.
12. Hochella JMF, Carim AH. *Surface science letters: A reassessment of electron escape depths in silicon and thermally grown silicon dioxide thin films*. *Surface Science*. 1988;197:L260-L8.
13. Yano F, Hiraoka A, Itoga T, Kojima H, Kanehori K, Mitsui Y. X-ray photoelectron spectroscopy study of submonolayer native oxides on HF-treated Si surfaces. *Journal of Vacuum Science & Technology: Part A-Vacuums, Surfaces & Films*. 1995;13(6):2671.
14. Lu ZH, McCaffrey JP, Brar B, Wilk GD, Wallace RM, Feldman LC, et al. SiO₂ film thickness metrology by x-ray photoelectron spectroscopy. *APPLIED PHYSICS LETTERS*. 1997;71(19):2764-6.
15. Fulghum JE. Determination of overlayer thickness by angle-resolved XPS: A comparison of algorithms. *Surface & Interface Analysis: SIA*. 1993;20(2):161.
16. Flitsch R, Raider SI. Electron mean escape depths from x-ray photoelectron spectra of thermally oxidized silicon dioxide films on silicon. *Mittlere Elektronenaustrittstiefen aus Photoelektronenspektren mit Roentgenstrahlen von thermisch oxidierten Siliciumdioxidduennschichten auf Silicium*. 1975(1):305.

Supplemental information

Part 1: Summary of all samples

Overview samples

solution	Date	Polymer	HAuCl ₄	Solvent	Additives	Dip-coating/Drop-casting	AFM	DLS	Comments
# 794	12/11/2013	185000-90000 24,90 mg	x	"original" Toluene 5 ml	x	18/11/2013 - Si - 7 V x3 18/11/2013 - APTES - 7 V x1	18/11/2013 - "nice" array - 27 nm	x	Original toluene was used
# 802	19/11/2013	185000-90000 25,23 mg	x	Toluene 5 ml	x	09/12/2013 - Si - 7 V x2	09/12/2013 - no micelles	x	Polymer layer
# 808	9/12/2013	185000-90000 25,10 mg	x	Toluene 5 ml	x	12/12/2013 - Si - 7 V x2 16/12/2013 - Si - 7 V x2	16/12/2013 - no micelles	x	Polymer layer
# 809	9/12/2013	185000-90000 24,98 mg	x	Toluene 5 ml	x	12/12/2013 - Si - 7 V x2 16/12/2013 - Si - 7 V x3	16/12/2013 - no micelles	x	Polymer layer
# 810	20/12/2013	185000-90000 24,95 mg	x	Toluene 5 ml	x	07/01/2014 - Si - 7 V x2	06/01/2014 - no micelles	x	Polymer layer
# 811	21/12/2013	185000-90000 25,05 mg	x	Toluene 5 ml	Methanol 50 µl	07/01/2014 - Si - 7 V x2	07/01/2014 - no micelles	x	Polymer layer
# 813	6/01/2014	185000-90000 25,05 mg	x	Toluene 5 ml	x	9/01/2014 - Si - 7 V x2 13/01/2014 - Si - 7 V x2	09/01/2014 - no micelles 13/01/2014 - no micelles	x	New polymer was used - Polymer layer
# 814	7/01/2014	185000-90000 25,17 mg	13/01/2014 0,5	Toluene 5 ml	x	9/01/2014 - Si - 7 V x2 13/01/2014 - Si - 7 V x2 16/01/2014 - Si - 7 V x2	13/01/2014 - no micelles 16/01/2014 - wide array - 73 nm	x	
# 815	13/01/2014	185000-73000 25,10 mg	31/01/2014 0,1	Toluene 5 ml	Methanol 50 µl	16/01/2014 - Si - 7 V x2	16/01/2014 - no micelles	x	Polymer layer Methanol was used to dissolve HAuCl ₄
# 816	13/01/2014	175000-70000 25,00 mg	31/01/2014 0,1	Toluene 5 ml	Methanol 50 µl	16/01/2014 - Si - 7 V x2	16/01/2014 - no micelles	x	Polymer layer Methanol was used to dissolve HAuCl ₄
# 817	13/01/2014	50000-16500 24,90 mg	31/01/2014 0,1	Toluene 5 ml	Methanol 50 µl	16/01/2014 - Si - 7 V x2	16/01/2014 - no micelles	x	Polymer layer Methanol was used to dissolve HAuCl ₄
# 818	17/01/2014	185000-90000 25,03 mg	31/01/2014 0,1	"wet" Toluene 5 ml	Methanol 50 µl	20/01/2014 - Si - 7 V x2 05/03/2014 - Si - 7 V x2	20/01/2014 - no micelles	x	"wet" toluene was used Methanol was used to dissolve HAuCl ₄
# 819	17/01/2014	185000-90000 25,01 mg	31/01/2014 0,1	"wet" Toluene 5 ml	Methanol/MiliQ 50 µl/50 µl	20/01/2014 - Si - 7 V x2 05/03/2014 - Si - 7 V x2	20/01/2014 - no micelles	x	Agglomerations of polymer "wet" toluene was used Methanol was used to dissolve HAuCl ₄
# 820	20/01/2014	185000-90000 24,95 mg	30/01/2014 0,1	Toluene (chem. dep.) 5 ml	Methanol 50 µl	23/01/2014 - Si - 7 V x2 03/02/2014 - Si - 7 V x2	23/01/2014 - no micelles 03/02/2014 - no micelles	x	Dry toluene from the chemistry departement was used Methanol was used to dissolve HAuCl ₄
# 823	24/01/2014	185000-90000 25,22 mg	30/01/2014 0,1	O-Xylene 5 ml	Methanol 50 µl	27/01/2014 - Si - 7 V x2 03/02/2014 - Si - 7 V x2 26/02/2014 - Si - 7 V x2	03/02/2014 - dens array - 29 nm 26/02/2014 - nice array - 44 nm	x	O-xylene was used, prior to filtration the solution looked "cloudy" and had some flakes in it (undissolved polymer?)
# 824	28/01/2014	185000-90000 25,02 mg	30/01/2014 0,1 03/02/2014 0,2 (total)	Toluene 5 ml	Methanol 50 µl	03/02/2014 - Si - 7 V x2 06/02/2014 - Si - 5 V x2	03/02/2014 - array - 23 nm	x	03/02/2014 - less symmetric as # 823
# 825	28/01/2014	248000-195000 25,00 mg	30/01/2014 0,1 03/02/2014 0,2 (total)	Toluene 5 ml	Methanol 50 µl	03/02/2014 - Si - 7 V x2 06/02/2014 - Si - 5 V x2	03/02/2014 - array - 33 nm	x	

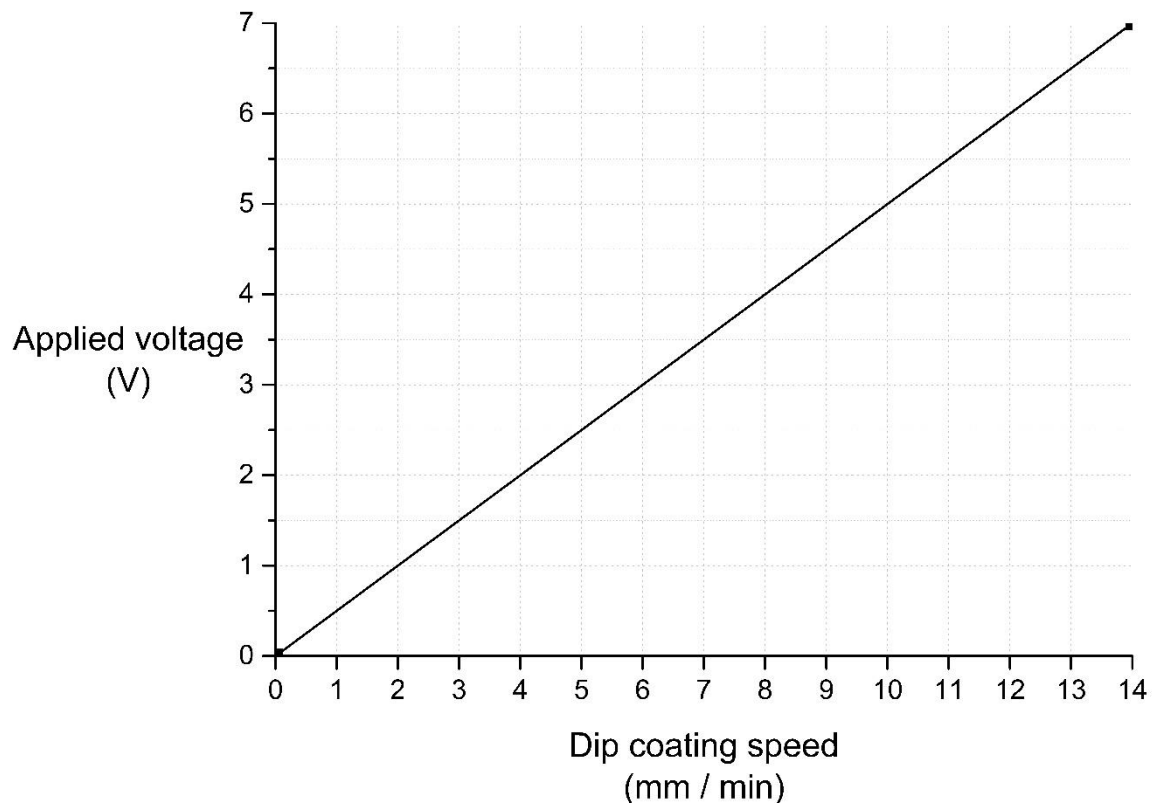
Overview samples

solution	Date	Polymer	HAuCl4	Solvent	Additives	Dip-coating/Drop-casting	AFM	DLS	Comments
# 830	11/02/2014	248000-195000 25,00 mg	12/02/2014 0,1 18/02/2014 0,2 (total)	O-xylene 5 ml	x	17/02/2014 - Si - 7 V x2 26/02/2014 - Si - 7 V x2	17/02/2014 - dens array - 55 nm 26/02/2014 - no micelles	x	
# 831	6/03/2014	32500-7800 25,49 mg	14/03/2014 0,5	Toluene 5 ml	x	x	x	11/03/2014 no micelles	
# 832	6/03/2014	185000-90000 25,32 mg	14/03/2014 0,5	Toluene 5 ml	x	x	x	11/03/2014 no micelles	only 1,8 ml was left after DLS
# 837	14/03/2014	32500-7800 25,17 mg	x	Toluene 5 ml	Methanol 50 µl	x	x	18/03/2014 no micelles	
# 838	14/03/2014	185000-90000 25,08 mg	x	Toluene 5 ml	Methanol 200 µl	x	x	18/03/2014 no micelles	
# 839	20/03/2014	185000-90000 24,99 mg	24/03/2014 0,5	Toluene 5 ml	x	28/03/2014 - APTES - 3 V x2 08/04/2014 - Si - 3 V x1 08/04/2014 - Si - 1 V x1 08/04/2014 - APTES - 3 V x1 08/04/2014 - APTES - 1V x1	28/03/2014 - wide array - 35 nm	x	
# 840	31/03/2014	32500-7800 25,00 mg	x	Toluene 5 ml	Methanol 200 µl	x	x	04/04/2014 no micelles	
# 841	31/03/2014	32500-7800 25,20 mg	x	Toluene 5 ml	Methanol 500 µl	x	x	04/04/2014 no micelles	
# 842	1/04/2014	32500-7800 25,22 mg	x	Toluene 5 ml	Methanol/MiliQ 150 µl/50 µl	04/04/2014 - APTES - 3 V x3	07/04/2014 - no micelles	04/04/2014 450 kcps - 48 nm 08/04/2014 no micelles	Solutions were sonicated for 1 h prior to DLS measurements 04/04/2014 - solution was filtered prior to dip-coating
# 843	7/04/2014	32500-7800 25,22 mg	x	Toluene 5 ml	Methanol/MiliQ 150 µl/50 µl	07/04/2014 - Si - 3 V x2	07/04/2014 - no micelles	08/04/2014 410 kcps - 45 nm	Solutions were sonicated for 1 h prior to dip-coating and DLS measurements 07/04/2014 - wetting problem?
# 844	8/04/2014	185000-90000 25,05 mg	08/04/2014 0,5	Toluene 5 ml	x	x	x	x	
# 846	10/04/2014	32500-7800 25,11 mg	x	Toluene 5 ml	Methanol/MiliQ 150 µl/20 µl	11/04/2014 - Si - 1 V x1 11/04/2014 - APTES - 1 V x1 11/04/2014 - Si - 1 cm x1 11/04/2014 - APTES - 1 cm x1	11/04/2014 - ?	x	Solutions were sonicated for 1 h prior to dip-coating and drop-casting
# 847	11/04/2014	32500-7800 25,08 mg	x	Toluene 5 ml	Methanol/Ethanol 150 µl/30 µl	11/04/2014 - Si - 1 V x1 11/04/2014 - APTES - 1 V x1 11/04/2014 - Si - 1 cm x1 11/04/2014 - APTES - 1 cm x1	11/04/2014 - ?	x	Solutions were sonicated for 1 h prior to dip-coating and drop-casting
# 848	11/04/2014	32500-7800 25,11 mg	x	Toluene 5 ml	Methanol/Ethanol 50 µl/100 µl	11/04/2014 - Si - 1 V x1 11/04/2014 - APTES - 1 V x1 11/04/2014 - Si - 1 cm x1 11/04/2014 - APTES - 1 cm x1	11/04/2014 - ?	x	Solutions were sonicated for 1 h prior to dip-coating and drop-casting
# 849	11/04/2014	32500-7800 25,11 mg	x	Toluene 5 ml	Methanol/Ethanol 150 µl/150 µl	11/04/2014 - APTES - 1 V x1 11/04/2014 - APTES - 1 cm x1	11/04/2014 - ?	x	Solutions were sonicated for 1 h prior to dip-coating and drop-casting

Overview samples

solution	Date	Polymer	HAuCl4	Solvent	Additives	Dip-coating/Drop-casting	AFM	DLS	Comments
# 852	25/04/2014	32500-7800 24,83 mg	x	Toluene 5 ml	20,00 mg P2VP 5000 in 100 µl Methanol	28/04/2014 - Si - 3 V x2 28/04/2014 - Si - 1 cm x1	28/04/2014 - wetting problem?	x	28/04/2014 - special US treatment (1/8", 65%, 30s pulse, 20s pause, 1min, 1min break, 1 min, 1ice cooled) Substrates were not cleaned
# 853	25/04/2014	185000-90000 24,93 mg	x	Toluene 5 ml	20,04 mg P2VP 5000 in 100 µl Methanol	28/04/2014 - Si - 3 V x2 28/04/2014 - Si - 1 cm x2	28/04/2014 - wetting problem?	x	28/04/2014 - special US treatment (1/8", 65%, 30s pulse, 20s pause, 1min, 1min break, 1 min, 1ice cooled) Substrates were not cleaned
# 854	30/04/2014	185000-90000 25,12 mg	30/04/2014 0,1	Toluene 5 ml	x	05/05/2014 - Si - 3 V x4	05/05/2014 - small micelles	x	
# 855	30/04/2014	185000-90000 25,12 mg	30/04/2014 0,2	Toluene 5 ml	x	05/05/2014 - Si - 3 V x1	05/05/2014 - small micelles	x	
# 856	9/05/2014	248000-195000 24,91 mg	09/05/2014 0,1	Toluene 5 ml	x	12/05/2014 - Si - 3 V x1	12/05/2014 - micelles wetting problem?	x	AFM deformed images?
# 857	9/05/2014	248000-195000 24,94 mg	09/05/2014 0,1	O-Xylene 5 ml	x	12/05/2014 - Si - 3 V x1	12/05/2014 - micelles	x	AFM deformed images?
# C4	14/02/2014	82000-83000 26,30 mg	x	Toluene 5 ml	x	25/02/2014 - Si - 10 mm/min x2	25/02/2014	11/03/2014 no micelles	Solution prepared by the chemistry department
# C5	14/02/2014	172000-42000 26,30 mg	x	Toluene 5 ml	x	25/02/2014 - Si - 10 mm/min x2	25/02/2014	11/03/2014 no micelles	Solution prepared by the chemistry department
# C6	14/02/2014	185000-73000 25,60 mg	x	Toluene 5 ml	x	25/02/2014 - Si - 10 mm/min x2	25/02/2014	11/03/2014 no micelles	Solution prepared by the chemistry department

Part 2: Speed voltage correlation of the dip coating setup



Auteursrechtelijke overeenkomst

Ik/wij verlenen het wereldwijde auteursrecht voor de ingediende eindverhandeling:

Electrostatic positioning of fluorescent nanodiamonds into nanoscaled arrays using block copolymer-based nanolithography

Richting: **master in de biomedische wetenschappen-bio-elektronica en nanotechnologie**

Jaar: **2014**

in alle mogelijke mediaformaten, - bestaande en in de toekomst te ontwikkelen - , aan de Universiteit Hasselt.

Niet tegenstaand deze toekenning van het auteursrecht aan de Universiteit Hasselt behoud ik als auteur het recht om de eindverhandeling, - in zijn geheel of gedeeltelijk -, vrij te reproduceren, (her)publiceren of distribueren zonder de toelating te moeten verkrijgen van de Universiteit Hasselt.

Ik bevestig dat de eindverhandeling mijn origineel werk is, en dat ik het recht heb om de rechten te verlenen die in deze overeenkomst worden beschreven. Ik verklaar tevens dat de eindverhandeling, naar mijn weten, het auteursrecht van anderen niet overtreedt.

Ik verklaar tevens dat ik voor het materiaal in de eindverhandeling dat beschermd wordt door het auteursrecht, de nodige toelatingen heb verkregen zodat ik deze ook aan de Universiteit Hasselt kan overdragen en dat dit duidelijk in de tekst en inhoud van de eindverhandeling werd genotificeerd.

Universiteit Hasselt zal mij als auteur(s) van de eindverhandeling identificeren en zal geen wijzigingen aanbrengen aan de eindverhandeling, uitgezonderd deze toegelaten door deze overeenkomst.

Voor akkoord,

Freiwald, Christopher

Datum: **10/06/2014**